JGR Atmospheres

RESEARCH ARTICLE
10.1029/2025JD044894

Special Collection:
Extratropical Large-scale Atmospheric Circulation Variability and Extreme Events Across Scales: Understanding, Modeling, and Prediction

All-Season Analysis of Extratropical and Arctic Cyclones Over the Northern Hemisphere Oceans During 1940–2024

Zhi-Bo Li[1], **Céline Heuzé**[1], **Jia-Ning Song**[2], **Alex Crawford**[3], **Hui-Wen Lai**[1], and **Deliang Chen**[4]

[1]Department of Earth Sciences, University of Gothenburg, Gothenburg, Sweden, [2]National Meteorological Centre, China Meteorological Administration, Beijing, China, [3]Department of Environment and Geography, University of Manitoba, Winnipeg, MB, Canada, [4]Department of Earth System Science, Tsinghua University, Beijing, China

Key Points:

- Arctic cyclogenesis has decreased in winter but increased in summer; spring cyclones are now more intense and longer-lived
- Cyclone tracks over the North Atlantic and North Pacific have lengthened, with more storms reaching the Arctic —especially in autumn and winter
- Arctic sea-ice loss enhances lower-level baroclinicity and weakens upper-level PV, reducing jet constraint on poleward cyclone migration

Supporting Information:

Supporting Information may be found in the online version of this article.

Correspondence to:

C. Heuzé and D. Chen,
celine.heuze@gu.se;
deliangchen@tsinghua.edu.cn

Citation:

Li, Z.-B., Heuzé, C., Song, J.-N., Crawford, A., Lai, H.-W., & Chen, D. (2026). All-season analysis of extratropical and arctic cyclones over the Northern Hemisphere oceans during 1940–2024. *Journal of Geophysical Research: Atmospheres*, *131*, e2025JD044894. https://doi.org/10.1029/2025JD044894

Received 17 JUL 2025
Accepted 26 FEB 2026

Author Contributions:

Conceptualization: Zhi-Bo Li, Céline Heuzé, Deliang Chen
Formal analysis: Zhi-Bo Li, Jia-Ning Song
Funding acquisition: Céline Heuzé, Deliang Chen

Abstract

Extratropical and Arctic cyclones regulate mid-to-high-latitude climate through the transport of heat, moisture, and momentum; however, their long-term behavior during spring and autumn seasons remains poorly understood. Using an 85-year (1940–2024) cyclone climatology derived from ERA5 reanalysis, we identified substantial seasonal and basin-specific shifts in Northern Hemisphere marine cyclone activity. Most notably, cyclone occurrence and intensity have significantly changed over the central Arctic Ocean, with winter storms becoming fewer but markedly deeper, and summer storms more numerous. Arctic cyclones in spring, previously under-investigated, have intensified (-0.31 hPa decade^{-1}) and exhibit lengthening lifespans ($+0.02$ days decade^{-1}) and trajectories ($+29.44$ km decade^{-1}). In the North Atlantic, cyclone paths have lengthened in winter, genesis has risen ($+0.73$ decade^{-1}) in spring, and storm lifespan has lengthened ($+0.03$ days decade^{-1}) in autumn. In the North Pacific, tracks also have lengthened in winter, while autumn storms have become larger ($+10.37$ km decade^{-1}), longer lived ($+0.03$ days decade^{-1}), and farther traveled ($+30.35$ km decade^{-1}). These observed cyclone changes are closely tied to the coupled responses from surface to upper-tropospheric levels. Pronounced sea ice loss coincides with enhanced lower-tropospheric baroclinicity (increased Eady growth rate) and a weaker upper-tropospheric potential vorticity gradient. Together, these adjustments favor stronger, deeper cyclones and facilitate their meridional propagation. Our results demonstrate that long-term climate change is reshaping Northern Hemisphere cyclone characteristics far beyond traditionally emphasized seasons. These findings highlight an urgent need for seasonal climate forecasts and long-term projections to give spring and autumn cyclones equal consideration alongside winter and summer extremes.

Plain Language Summary

Extratropical and Arctic cyclones play an important role in shaping climate, ecosystems, and human activities. These storms help move heat and moisture toward the poles and affect sea ice, ocean waves, coastal flooding, and marine transportation. While past research has mostly focused on changes in cyclones during winter and summer, much less attention has been given to the transitional seasons —spring and autumn. In this study, we analyzed long-term weather data from 1940 to 2024 to examine how cyclones over the Northern Hemisphere oceans have changed across all seasons. We found clear and important seasonal shifts. In the Arctic, spring cyclones are now stronger, last longer, and travel farther. In the North Atlantic, more cyclones are forming in spring, and autumn storms are lasting longer. Similar trends appear in the North Pacific, where autumn storms are becoming larger, longer-lived, and more wide-ranging. These changes are closely linked to the loss of Arctic sea ice. As ice retreats, the temperature contrast between the ocean and atmosphere increases, creating favorable conditions for stronger storm development. Our findings highlight the need for seasonal forecasts and climate models to pay more attention to spring and autumn cyclones—not just those in winter and summer.

1. Introduction

Extratropical and Arctic cyclones are the primary synoptic-scale engines that redistribute heat, moisture, and momentum across the mid- and high-latitude Northern Hemisphere. By carving the canonical North Atlantic and North Pacific storm tracks, they ventilate the upper ocean, mix trace gases, and deliver many of the wind-wave events that shape coastal risk (Bengtsson et al., 2006; Feser et al., 2014; Hoskins & Hodges, 2002; Ulbrich et al., 2009). Because the poleward energy flux carried by cyclones rivals that of the mean meridional circulation (Lembo et al., 2019, 2022; Messori & Czaja, 2012; Stoll et al., 2023), even modest, sustained shifts in their

Investigation: Zhi-Bo Li, Alex Crawford
Methodology: Zhi-Bo Li, Jia-Ning Song, Alex Crawford
Software: Zhi-Bo Li, Alex Crawford
Supervision: Céline Heuzé, Deliang Chen
Visualization: Zhi-Bo Li
Writing – original draft: Zhi-Bo Li
Writing – review & editing: Céline Heuzé, Jia-Ning Song, Alex Crawford, Hui-Wen Lai, Deliang Chen

frequency, depth, or preferred pathway can cascade through the climate system, altering sea-ice export, air–sea CO_2 exchange, storm surge, extreme wind and rainfall (Barnes & Screen, 2015; Chen et al., 2023; IPCC, 2022; Raible et al., 2020). Therefore, a robust historical assessment of where, when, and how seasonal cyclones have changed remains a cornerstone for credible climate-change attribution and projection.

Objective storm-tracking studies conducted over the modern reanalysis era reveal rich multidecadal variability in extratropical cyclone behaviors, including occurrence frequency, strength, lifespan, pathway, etc. (e.g., Feser et al., 2014; Raible et al., 2018). A pioneering comparison of the 40-year European Centre for Medium-Range Weather Forecasts Re-Analysis (ERA-40) with the National Centers for Environmental Prediction/National Center for Atmospheric Research (NCEP–NCAR) data set documented a 10%–20% rise in strong winter cyclones and a northeastward shift of the North Atlantic track between 1958 and 2001 (Wang et al., 2006). The community experiment Intercomparison of Mid-Latitude Storm Diagnostics (IMILAST) later showed that such trends are robust to detection-scheme choice, despite methodological spread in weaker systems (Neu et al., 2013). Wickström et al. (2020) reported poleward shifts of high-latitude North Atlantic cyclone occurrence during 1979–2016, which was also found in multiple climate model simulations (Dzambo et al., 2023; Priestley & Catto, 2022). However, Hay et al. (2023) reported that the North Atlantic storm track shifted southward in winter. Using the back-extended ECMWF Reanalysis v5 (ERA5), Karwat et al. (2022) found statistically significant winter strengthening and longer lifespans of extratropical cyclones in the North Pacific and North Atlantic from 1950 to 2021. Karwat et al. (2022) also found increasing trends of the Northern Hemisphere (NH) cyclonic travel distance with a slower deepening rate.

Arctic cyclones exhibit equally pronounced seasonality. An earlier work by Zhang et al. (2004) proposed that there was an increasing trend of Arctic cyclone numbers during 1948–2002, especially in summer. Trajectory studies reveal that deep Arctic cyclones have become more frequent since 1948, even as weaker systems have declined (Sepp & Jaagus, 2011; Serreze & Barrett, 2008; Simmonds et al., 2008). A multi-reanalysis comparison demonstrated that these signals persist when cyclone radii are standardized (Zahn et al., 2018). Recently, Zhang et al. (2023) documented a significant deepening and lengthening of Arctic cyclone lifespans during 1950–2021, with the most explosive events almost doubling in frequency. In particular, extreme Arctic cyclones have been reported during the recent decades (Simmonds & Rudeva, 2012; Tao et al., 2017). Moreover, Zhang et al. (2023) also highlighted that the spatial center of strong Arctic cyclones has shifted poleward in winter and summer.

The physical mechanisms of long-term, mid-high-latitude cyclone variability are multifaceted. Classical baroclinic-instability theory expresses growth through the maximum Eady growth rate (EGR), which combines vertical wind shear and static stability (Eady, 1949), which indicates how conducive the environment is to cyclone genesis and deepening (Hoskins & Valdes, 1990; Pierrehumbert & Swanson, 1995). Crawford et al. (2022) showed that low sea-ice regimes accelerate local winter storm deepening in the Arctic by enhancing turbulent heat fluxes and reducing static stability while enhancing low-level baroclinicity. However, at a larger scale, declining sea-ice concentration may weaken extratropical cyclone development via reductions in upper-level wind shear (Blackport & Screen, 2020; Francis & Vavrus, 2012; Vihma, 2014). Dynamical adjustments—e.g., a poleward drift of the eddy-driven jet (Hermoso et al., 2024; Yin, 2005), faster downstream development linked to enhanced storm propagation (Tamarin-Brodsky & Kaspi, 2017), and coupling between stratosphere and tropopause polar vortices (Gray et al., 2021; Simmonds & Rudeva, 2014)—would help explain the cyclonic track shifts. Besides, decadal shifts of atmospheric and oceanic oscillations play roles in modulating Arctic cyclone statistics, including the Arctic Oscillation (Simmonds et al., 2008; Wang et al., 2006), Beaufort Gyre (Kenigson & Timmermans, 2021), and El Niño Southern Oscillation (Rinke et al., 2017).

Two major limitations emerge from previous studies. First, most analyses target extratropical and Arctic cyclones in winter and summer, while transitional seasons remain under-explored, leaving uncertainty in the full scope of cyclone evolution. Second, extratropical and Arctic cyclones are rarely assessed together under a unified cyclone tracking methodology, obscuring basin-to-basin comparisons. To isolate cyclones whose formation is most directly influenced using oceanic processes and sea-ice variability, we restrict the genesis statistics to storms that first form over the ocean. This reduces the influence of land-based baroclinic zones, orographic effects, and land–atmosphere coupling. We acknowledge that continents can also host strong baroclinic zones and generate intense cyclones that later enter the Arctic, but these land-genesis storms are not the focus here (Simmonds & Li, 2021). Our results therefore represent a marine-genesis subset of the full cyclone spectrum. Our study addresses these knowledge gaps with an 85-year (1940–2024) cyclone atlas derived from the ERA5 reanalysis (Hersbach

et al., 2020). To make the contribution relative to prior work explicit, we assessment that (a) resolves the full seasonal cycle, including the spring and autumn transition seasons that are often merged or omitted; (b) spans an 85-year period that allows recent multi-decadal changes to be interpreted against longer-term variability; and (c) evaluates extratropical and Arctic cyclones together across the Northern Hemisphere oceans using consistent metrics (track density, occurrence, intensity, size, lifespan, and track length), enabling basin-to-basin and Arctic–midlatitude contrasts. This broader scope also allows us to connect the seasonally dependent cyclone changes to concurrent changes in baroclinicity, sea-ice concentration, and upper-level potential vorticity gradients within a coherent framework. The paper structure is as follows: Section 2 describes the data and methodology; Section 3 presents the detailed spatial-temporal evolution of extratropical and Arctic cyclones; Physical mechanisms and limitations are discussed in Section 4; and Section 5 summarizes the conclusions and gives the broader implications.

2. Data Sets and Methodologies

2.1. Atmospheric Reanalysis

Atmospheric variables were derived from the ERA5 data set (Hersbach et al., 2020), with a horizontal resolution of 0.25° × 0.25° and a temporal resolution of 6 hr (00, 06, 12, and 18 hr). The ERA5 uses a hybrid 4D-Var assimilation scheme, which includes more observational data sets, and has been widely used in investigating extratropical and Arctic cyclones in recent years (Crawford et al., 2022; Karwat et al., 2022; Song et al., 2021; Yu et al., 2022; Zhang et al., 2023, 2024). We used sea level pressure (SLP), air temperature, potential vorticity, and horizontal zonal and meridional winds from 1940 to 2024. Karwat et al. (2022) reported that midlatitude storm statistics in the pre-satellite extension of ERA5 back to 1950 are broadly consistent with those from the satellite era, supporting the use of ERA5 for multi-decadal storm-track studies.

Several studies have proposed that different reanalyses lead to similar results (Chang et al., 2016; Yu et al., 2022; Zahn et al., 2018; Zhang et al., 2023). To evaluate the robustness of the ERA5-based results, we also used JRA55 (Kobayashi et al., 2015) and NOAA-20 Century Reanalysis Version 3 (hereafter NOAA20C) (Slivinski et al., 2019). JRA55 has a horizontal resolution of ∼0.5625° (∼50 km), and NOAA20C is 1° (∼100 km). Both products are available at 6-hourly resolution, consistent with ERA5, which allows us to apply the same cyclone-tracking workflow and diagnostics across data sets. Because NOAA20C ends in 2015, we focus on the common period 1979–2015 for an internally consistent comparison.

2.2. Sea Ice Concentration

Monthly sea ice concentration is derived from the Hadley Centre Sea Ice and Sea Surface Temperature data set (HadiSST) (Rayner et al., 2003). This data set has a horizontal resolution of 1° × 1° for 1940–2024. Sea ice data are obtained from a variety of sources, including digitized sea ice charts and passive microwave retrievals. The sea ice fields are made more homogeneous by compensating satellite microwave-based sea ice concentrations for the impact of surface melt effects on retrievals in the Arctic, and by making the historical in situ concentrations consistent with the satellite data (Rayner et al., 2003).

2.3. Cyclone Detection and Tracking

Cyclones are detected with an updated version of the Lagrangian cyclone detection tracking algorithm introduced by Crawford and Serreze (2016), which was benchmarked against alternative schemes and grid resolutions by Crawford et al. (2021). Consistent with the optimal configuration in those experiments, we apply the tracker to 6-hourly SLP fields from the ERA5 on a 50 km polar stereographic grid; finer sampling (<3 hr) tends to split fast-moving storms, whereas coarser sampling or grids >100 km miss a substantial fraction of short-lived systems.

A SLP minimum is accepted as a cyclone "seed" only if it satisfies three geometric and topographic filters that have proved robust in earlier sensitivity tests (Crawford et al., 2021):

1. Local minimum criterion—The candidate's SLP is lower than that at every grid point within ±200 km in both zonal and meridional directions (a 400 km × 400 km kernel).
2. Background-gradient criterion—The azimuthal-mean SLP within a 1,000 km radius exceeds the candidate value by at least 7.5 hPa, filtering out shallow thermal lows.

3. Topographic criterion—The grid cell lies below 1,500 m and at least 60% of the cells inside the 200 km kernel are also below that elevation, preventing spurious minima over steep terrain.

For each accepted center, the initial cyclone envelope is the outermost closed isobar that encloses the minimum and no SLP maxima. If two centers are separated by <1,200 km, their envelopes are compared; when merging the envelopes increases the area of the larger system by a factor of two or more, the pair is reclassified as a single multi-center cyclone. Tracks are updated every 3 hr. A linear extrapolation from the two previous positions provides a first-guess location; the candidate center at the next time step that lies closest to this position and within 450 km of the prior center is selected as the continuation of the track. The 450 km threshold corresponds to a maximum translation speed of 150 km hr^{-1} is sufficient for the fastest observed cyclones yet restrictive enough to avoid erroneous jumps. Tracks shorter than 24 hr or consisting of fewer than four positions are discarded.

Each cyclone is assigned to one of three genesis sectors—Arctic Ocean (65°N–90°N), North Atlantic (60°W–0°E, 30°N–65°N), or North Pacific (140°E−130°W, 30°N–65°N)—based solely on the first closed SLP minimum; storms that subsequently leave their sector remain classified by their origin (Figure S1 in Supporting Information S1). All cyclones that form south of 30°N are not detected as extratropical cyclones. Crawford et al. (2022) showed that this "first-footprint" rule captures the dominant surface-flux environment controlling the cyclonic early deepening.

2.4. Cyclone Metrics Definitions

Cyclone intensity is measured by the curvature of the sea-level pressure field (DsqP), defined as the area-weighted mean Laplacian (second derivative) of pressure over the cyclone footprint (Crawford et al., 2021; Crawford & Serreze, 2016; Serreze et al., 1997). Larger DsqP indicates a sharply curved pressure field and thus a more intense cyclone.

Cyclone depth is defined as the average difference in pressure between the storm center and the edge. The cyclone depth reflects the central pressure gradient relative to the environment, while cyclone intensity incorporates areal curvature and can capture more structural aspects of cyclone evolution (Crawford et al., 2021; Simmonds & Keay, 2000).

Cyclone radius is defined as the square root of the cyclone's area divided by π at each time step, while cyclone area is defined via the outermost closed isobar, meaning the isobar with the highest SLP that encloses the cyclone center of interest but no centers from other cyclones and no SLP maxima (Crawford et al., 2021).

2.5. Eady Growth Rate

The maximum EGR provides a first-order diagnosis of synoptic-scale baroclinic instability, and therefore of an environment's potential to foster cyclone genesis and rapid deepening (Eady, 1949; Hoskins & Valdes, 1990; Pierrehumbert & Swanson, 1995; Simmonds & Lim, 2009). Formally, EGR is the product of two atmospheric properties evaluated over a tropospheric layer: the Brunt–Väisälä frequency N, which represents static stability, and the magnitude of the vertical wind shear S:

$$\mathrm{EGR} = 0.3098\,\frac{S}{N} \tag{1}$$

Static stability is related to the vertical gradient of potential temperature:

$$N = \left(\frac{g}{\theta}\,\frac{\delta\theta}{\delta z}\right)^{0.5} \tag{2}$$

with g the acceleration of gravity, θ potential temperature, and z geometric height. The vertical shear of the horizontal wind (U) is:

$$S = \left| f\,\frac{\delta U_{(z)}}{\delta z} \right| \tag{3}$$

where f denotes the Coriolis parameter. Via the thermal-wind relationship, the shear term is directly proportional to the horizontal temperature gradient (Wallace & Hobbs, 2006).

In this study, 3-hourly EGR is evaluated from ERA5 fields on the 925, 850, and 700 hPa levels; then, the seasonal average of EGR is calculated. Focusing on these lower layers targets the portion of the troposphere most immediately affected by sea-ice changes and surface heat-flux anomalies (Rinke et al., 2006; Serreze et al., 2009). For each time step, the layer-maximum value is retained at every grid point, and seasonal means are then formed on the 50-km analysis grid.

3. Spatial-Temporal Evolution of Extratropical and Arctic Cyclones

3.1. Spatial Distributions of Cyclone Track and Density

In this section, we systematically analyze the seasonal characteristics of extratropical and Arctic cyclones, including winter (December–January–February, DJF), spring (March–April–May, MAM), summer (June–July–August, JJA), and autumn (September–October–November, SON). The reason we use standard meteorological seasons is that they separate the canonical winter storm-track regime, the spring transition, the summer minimum, and the autumn re-intensification. Extended season windows (e.g., NDJFM) can be useful for targeted applications, but they blend transition months and may mask season-specific signals.

Figure 1 shows the climatological cyclone track density from 1940 to 2024 and illustrates a systematic latitudinal reorganization of storm activity through the annual cycle. In winter (Figure 1a), two coherent storm-track maxima dominate the NH: (a) one extends from the Northwest Atlantic to the Barents Seas (North Atlantic storm track) and (b) the other spans the Northwest Pacific to the Gulf of Alaska (North Pacific storm track) (Hoskins & Hodges, 2002; Wernli & Schwierz, 2006). The hotspots over Ellesmere Island and the Alaska Range are artifacts in ERA5, which was also the case for ERA-Interim (Crawford & Serreze, 2016; Serreze & Barrett, 2008; Zhang et al., 2004). In spring (Figure 1b), mid-latitude densities decrease by ∼30%, and the spatial pattern is quite similar to that in winter (Figure 1a). The winter and spring maxima arise because baroclinicity and the eddy-driven jet are strongest in DJF and MAM. As the large-scale meridional temperature gradient weakens toward summer and the jet shifts poleward, cyclone development becomes less frequent, reducing midlatitude track density while maintaining a similar corridor structure (Chang et al., 2016; Hoskins & Hodges, 2002). Summer (Figure 1c) exhibits the minimum hemisphere-wide cyclone activity, with densities below 12 per 400 km^2 per season except the Icelandic Low region, where coastal baroclinicity sustains modest storm counts (Zahn et al., 2018). By autumn (Figure 1d), the Atlantic and Pacific storm tracks recovered to near the winter amplitudes. Collectively, these panels reveal a meridional displacement of the primary storm belt, reflecting the seasonal meridional expansion and contraction of the cyclones.

Relative trends (% per decade, normalized by climatology) in track density (Figure 2) demonstrate the changes in seasonal migration over the past 85 years. Winter trends (Figure 2a) show statistically significant increases of 4%–8% $decade^{-1}$ across the central Arctic Ocean, Barents–Kara Sea, and Beaufort–Chukchi sector, accompanied by concurrent decreases of 2%–6% $decade^{-1}$ in portions of the western North Atlantic, which indicates a poleward redistribution of extratropical cyclones. Spring (Figure 2b) continues the poleward reorganization, implying an earlier seasonal incursion of storms into the ice-covered basin. The strongest adjustments occur in summer (Figure 2c); cyclone track densities rise by more than 8% $decade^{-1}$ along the Siberian marginal-ice zone, as well as significant increasing trends over North Atlantic and North Pacific storm track regions. Autumn trends (Figure 2d) show enhanced activity over the central Arctic. The relatively scattered distribution of trend signals reflects the contribution of internal variability (Ulbrich et al., 2009). A poleward shift or slight zonal reorganization of a storm track produces bands of decreasing track density on its equatorward side and increasing density on its poleward side (Feser et al., 2014). The combination of Figures 1 and 2 indicates a year-round amplification of Arctic cyclone frequency since 1940.

Figure 3 describes the climatological cyclone intensity over 1940–2024. In winter (Figure 3a), the deepest systems (≥5 hPa per 50 km^2) are along the southern flank (∼40°N) of the principal North Pacific storm track, with relatively high intensity (≥4 hPa per 50 km^2) also found surrounding the Aleutian Low. A second high-amplitude zone of comparable magnitude spans from the Northwest Atlantic through the Icelandic-to-Greenland Sea sector, and northeastward. Intensities over the central Arctic Ocean are lower, generally 2–3 hPa per 50 km^2. During spring (Figure 3b), both mid-latitude cores weaken by ∼1 hPa, while a lobe of 2.5–3 hPa persists over the

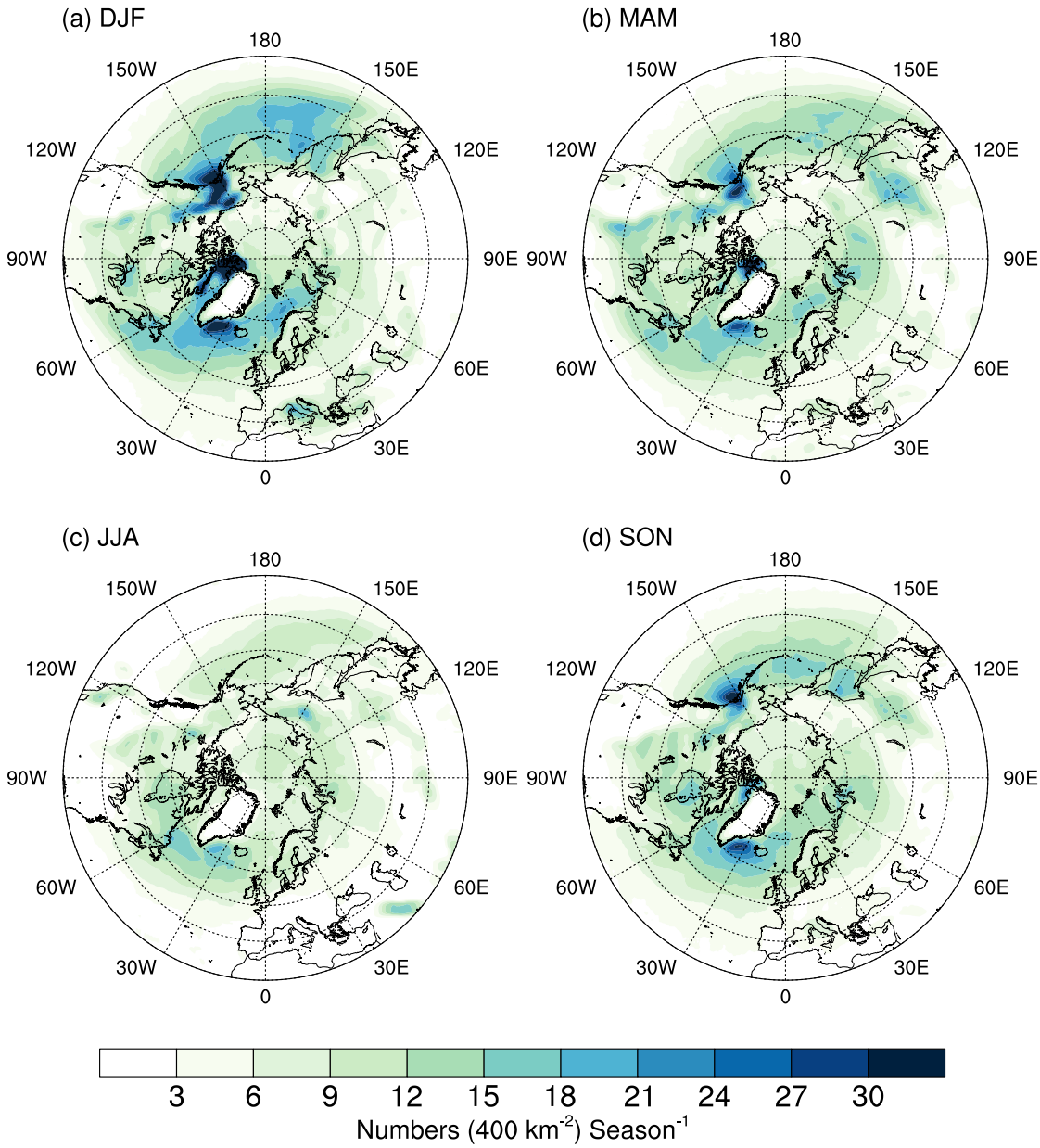

Figure 1. Spatial distributions of climatological (1940–2024) cyclone track density (numbers season^{-1}) of extratropical and Arctic cyclones in (a) winter (December–January–February), (b) spring (March–April–May), (c) summer (June–July–August), and (d) autumn (September–October–November), respectively.

Barents–Kara Sea. Summer (Figure 3c) exhibits the shallowest systems, with values rarely exceeding 2 hPa per 50 km^2, except along the storm track regions. The cyclone intensity rebounds sharply in autumn (Figure 3d). The North Pacific maximum re-intensifies to winter-like amplitudes, and the Atlantic–Arctic maximum reforms with much stronger amplitude than that in winter. Following the September ice minimum, large sensible and latent fluxes arise when cold air moves over newly exposed water. These fluxes steepen low-level air temperature gradients and enhance the EGR, as we will show in Section 4, favoring rapid cyclone intensification (Hsu et al., 2025; LeDrew, 1984; Serreze et al., 2009; Simmonds & Keay, 2009).

Figure 4 displays the relative trend in cyclone intensity, which supplements the previously poorly understood changes in cyclone intensity during the transition season. In winter (Figure 4a), a coherent intensification (1%–3% decade^{-1}) covers the central Arctic Ocean and extends southwestward into Baffin Bay, while an equally strong positive trend is located along the North Pacific storm track. This intensification is accompanied by

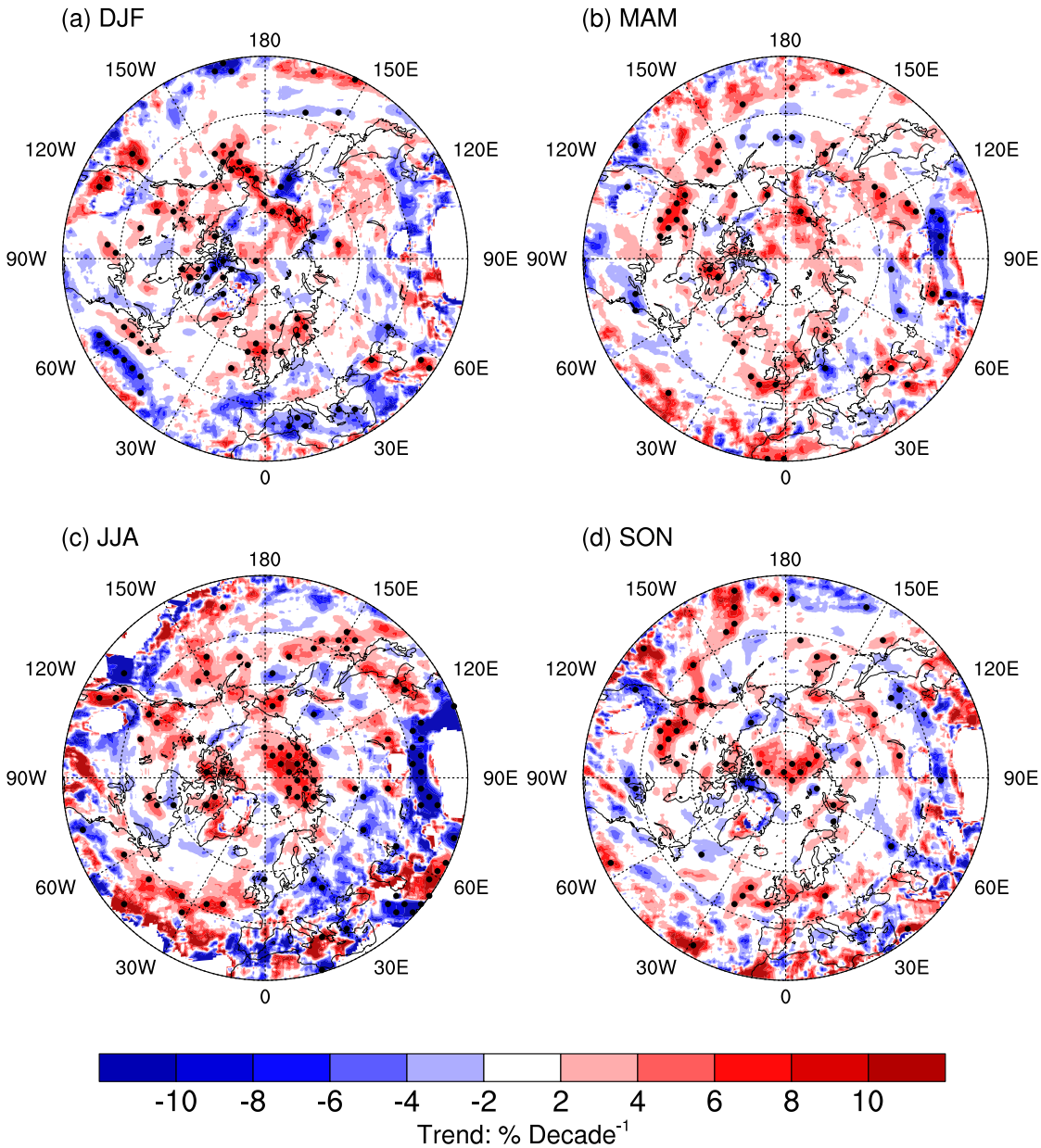

Figure 2. Spatial distributions of relative cyclone track density trend (trend/climatology) (% decade^{-1}) of extratropical and Arctic cyclones in (a) winter (DJF), (b) spring (MAM), (c) summer (JJA), and (d) autumn (SON), respectively. Black dots denote that the trends are significant at the 0.05 levels.

statistically significant weakening along the west coast of North America and over the seas south of Japan, indicating that the strongest systems tend to shift toward the central basin. In spring (Figure 4b), positive trends dominate the Northwest Pacific and Northeast Atlantic, whereas negative trends appear over the Bering Sea. Summer (Figure 4c) displays the most pronounced intensification pattern, with the intensity increases exceeding 3% decade^{-1} over most of the Arctic Ocean and nearly half of the North Pacific, while cyclone intensity weakens near the west coast of North America. By autumn (Figure 4d), positive trends still dominate the Arctic Ocean and the Northwest Pacific, while negative trends are mainly confined to the Hudson Bay and portions of the eastern North Pacific.

The cyclone depth climatology shares a similar distribution with that of the cyclone intensity (Figures S2 and S3 in Supporting Information S1). The relative trend of cyclone depth serves to validate and complement the intensity-based results in Figure 4. In particular, significant positive trends across the central Arctic, North

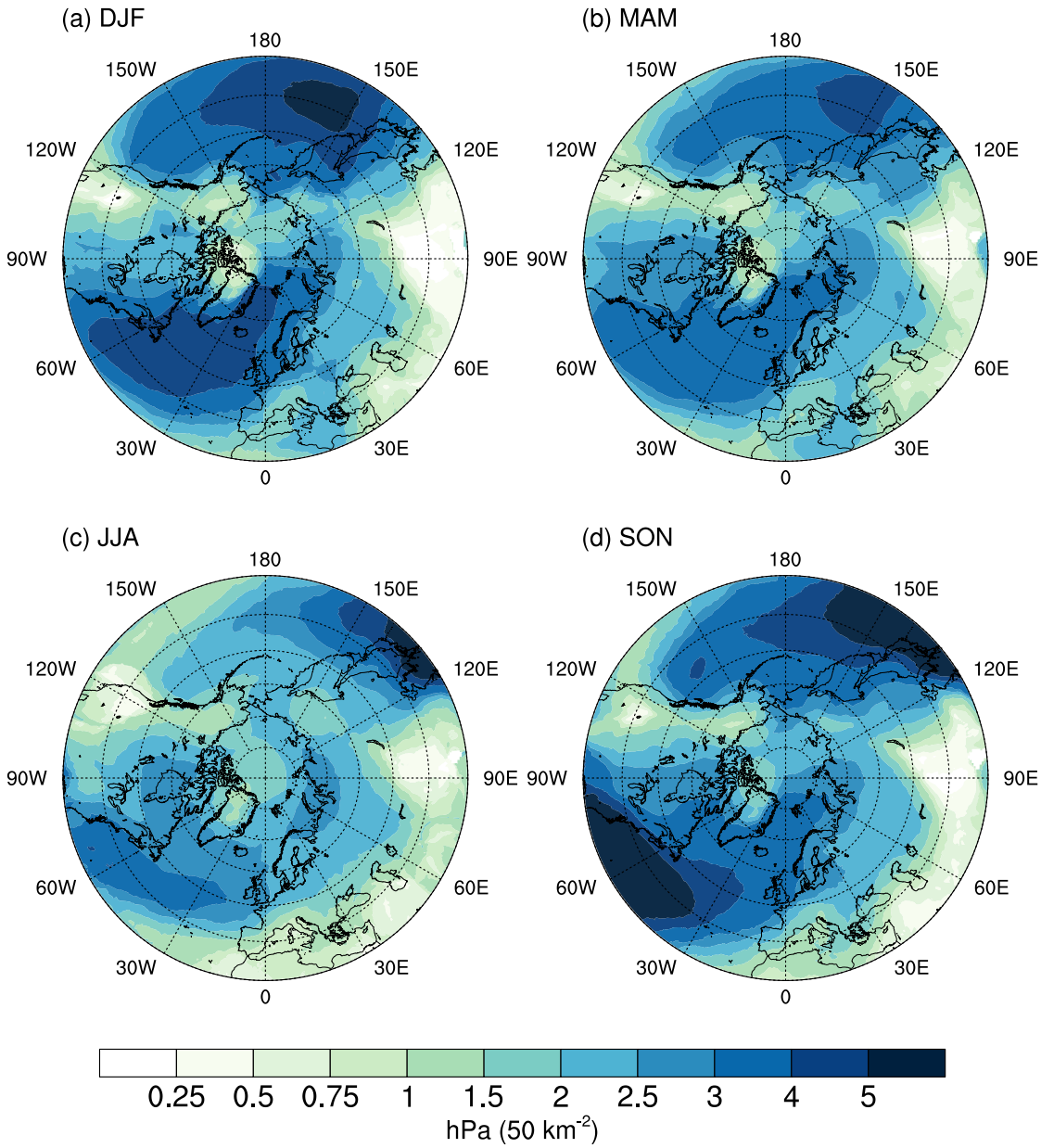

Figure 3. Spatial distributions of climatological (1940–2024) cyclone intensity (DsqP; the area-weighted mean Laplacian of pressure over the cyclone footprint) of extratropical and Arctic cyclones in (a) winter (DJF), (b) spring (MAM), (c) summer (JJA), and (d) autumn (SON), respectively.

Pacific, and Barents–Kara sector are evident across multiple seasons (Figures S3 and S4 in Supporting Information S1). Minor regional discrepancies exist—for example, in summer (Figure S3c in Supporting Information S1), depth trends are more spatially fragmented across the North Pacific and Arctic compared to intensity. Nonetheless, the general agreement between depth and intensity reinforces the conclusion of widespread Arctic and extratropical cyclone enhancement.

Figures S4–S6 in Supporting Information S1 show the climatological (1979–2015) spatial distributions of cyclone track density, cyclone density, and cyclone depth derived from ERA5, JRA55, and NOAA20C. Across all seasons, the three data sets exhibit a highly consistent large-scale structure: the main storm-track corridors and their seasonal migration are reproduced in each product, with maxima occurring in the same broad regions and with similar spatial extents. The expected seasonal cycle is also consistent, with generally stronger activity in the cold seasons and weaker activity in summer. There are smoother and slightly weaker gradients in NOAA20C,

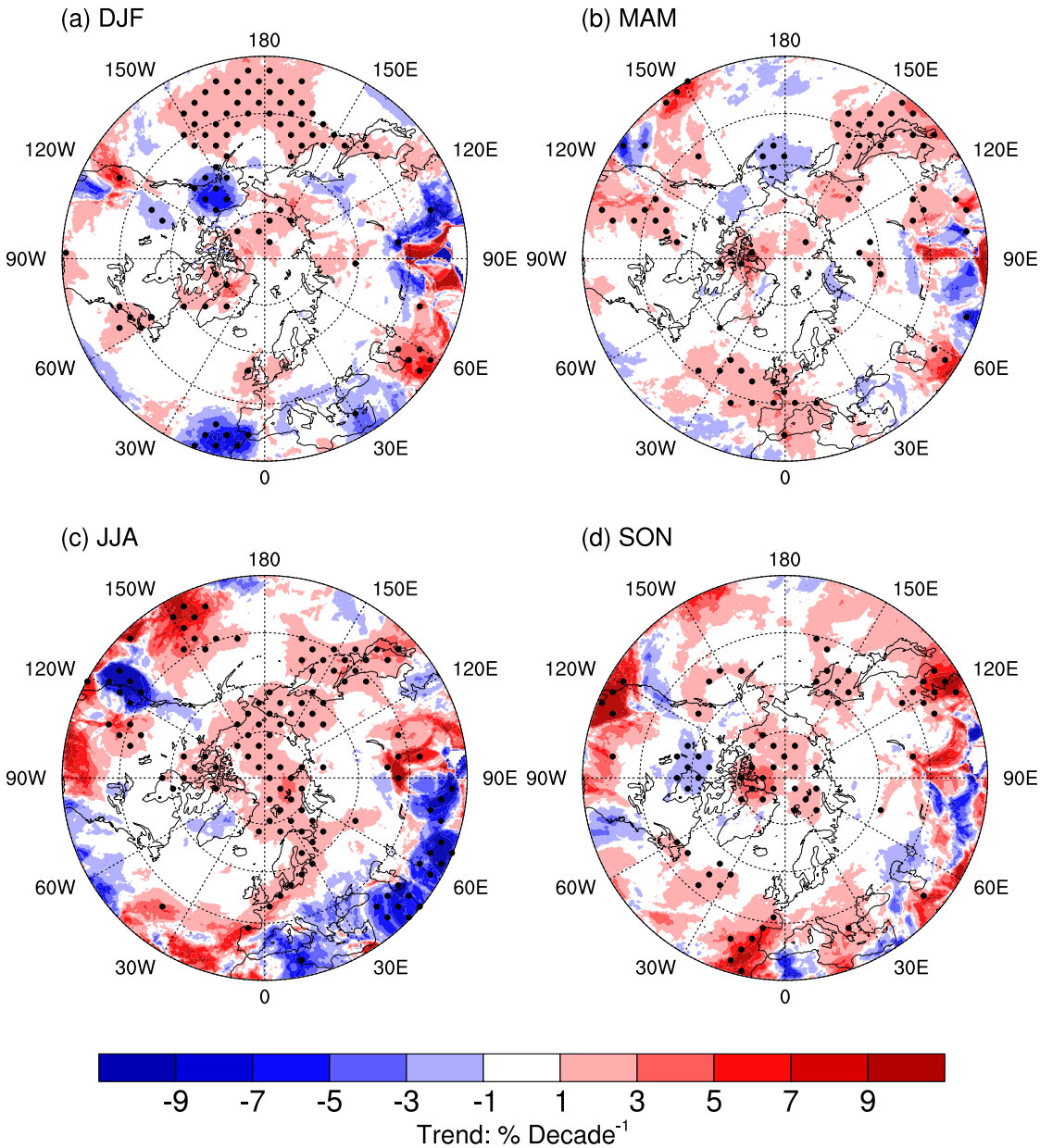

Figure 4. Spatial distributions of relative cyclone intensity trend (trend/climatology) (% decade^{-1}) of extratropical and Arctic cyclones in (a) winter (DJF), (b) spring (MAM), (c) summer (JJA), and (d) autumn (SON), respectively. Black dots denote that the trends are significant at the 0.05 levels.

which is expected given its coarser resolution, but these differences do not alter the spatial organization of cyclone activity. Figures S7–S9 in Supporting Information S1 provide the corresponding relative trend patterns. While trend maps are inherently more spatially heterogeneous and show some data set-to-data set variability at small scales, the three reanalyses still show broad agreement in the location and sign of the dominant, large-scale trend features, and regions highlighted as statistically robust tend to occur in comparable areas across data sets. These indicate that our conclusions are not dependent on a single reanalysis product.

Taken together, these season-specific patterns reveal a sustained enhancement of the Arctic cyclones. The North Pacific also experienced significant enhancement of extratropical cyclones, especially in winter and summer, while enhancement of extratropical cyclones in the North Atlantic favors the transition seasons, spring and autumn.

3.2. Temporal Evolution of Regional Cyclonic Metrics

To complement Section 3.1, we also consider the temporal changes of cyclone records grouped into the three genesis regions that dominate the NH oceans: the Arctic Ocean, North Atlantic, and North Pacific. To that end, Figure 5 through Figure 8 track four fundamental properties (seasonal generation count, lifespan, lowest central SLP, and trajectory length) across the 1940–2024 period.

Figure 5 shows that the seasonal frequency of cyclone genesis has evolved unevenly across the three oceans. For the Arctic (Figure 5a), winter remains the season with the largest cyclogenesis number (≈115 years^{-1}) but significantly decreases by −1.23 per decade ($P < 0.05$). Summer, by contrast, has a much lower genesis number (≈55 years^{-1}) but increases significantly by +0.95 per decade ($P < 0.01$). The spring and autumn series stay steady and have interannual fluctuations of ±15% of the climatology. This means that the long-term Arctic cyclogenesis shift involves a redistribution from the coldest to the warmest season rather than a uniform increase. In the North Atlantic (Figure 5b), winter has the largest genesis number (≈115 years^{-1}), followed in order by spring, autumn, and summer. Only spring exhibits a significantly increasing trend of +0.73 per decade ($P < 0.1$). The North Pacific (Figure 5c) generates more cyclones than either of the other basins in every season, but none of its seasonal series displays a significant linear trend and the interannual variabilities are less than those in other regions.

Figure 6 documents the seasonal mean lifespan of cyclones. For the Arctic (Figure 6a), winter cyclones are the shortest lived (≈3.3 days) and show no detectable trend, whereas the spring cyclones lengthen significantly by +0.02 days (about half an hour) per decade ($P < 0.05$). The lifespans in summer and autumn remain relatively stable, with large interannual fluctuations in summer from 3.3 to 5.4 days. The North Atlantic (Figure 6b) exhibits uniformly longer lifespans, but only autumn has a significant lengthening trend of +0.03 days per decade ($P < 0.1$), which equals to 6 hr longer lifespan in 85 years, and all the other seasons show weak lengthening trends. In the North Pacific (Figure 6c), only autumn cyclones display a significant lengthening of +0.03 days per decade ($P < 0.01$). Overall, these results indicate that cyclone lifespans for most seasons/regions are stable, but the only significant trends are toward cyclones persisting slightly longer, enhancing their capacity for sustained heat and momentum export.

Figure 7 summarizes the evolutions in the central SLP of seasonal cyclones. Arctic cyclones' central SLP are comparable across four seasons (Figure 7a), but the North Atlantic and North Pacific cyclones have the lowest central SLP in winter, followed by autumn, spring, and summer (Figures 7a and 7b). The Arctic cyclones (Figure 7a) have become significantly more intense in the winter by −0.28 hPa per decade ($P < 0.1$) and spring by −0.31 hPa per decade ($P < 0.05$). Neither the North Atlantic (Figure 7b) nor the North Pacific (Figure 7c) exhibits a season in which the trend approaches the 0.1 significance level. The absence of mid-latitude pressure changes supports the view that the intensification maxima in Figure 4 reflect poleward relocation of the deepest cyclones rather than basin-wide deepening.

Figure 8 describes the evolution of seasonal cyclone track length. Arctic (Figure 8a) spring cyclone trajectories increased by +29.44 km per decade ($P < 0.01$), consistent with the simultaneous increases in lifespan and intensity. Other seasons have no significant changes. The North Atlantic (Figure 8b) reveals a significant winter extension of +18.52 km per decade ($P < 0.1$), and autumn also has an increasing trend, even though it is not significant. The most pronounced enlargement occurs in the North Pacific (Figure 8c), with autumn tracks significantly lengthening by +30.35 km per decade ($P < 0.01$), and winter tracks by +6 km per decade ($P < 0.1$). The ratio of travel distance to lifespan can approximate the translation speed. Figure S10 in Supporting Information S1 shows that translation-speed trends are weak compared to the changes in travel distance and lifetime, and they are not spatially uniform. The Arctic shows an insignificant increase, while the North Atlantic and North Pacific show increased speed in DJF and MAM but decreased speed in JJA and SON.

Besides, we examined the latitude of genesis and lysis together with cyclone size (Figures S11–S13 in Supporting Information S1). These additional diagnostics reveal only a few statistically robust changes. In the North Atlantic, the summer genesis belt (Figure S11b in Supporting Information S1) significantly drifted equatorward by about 0.10° latitude per decade and the corresponding lysis belt (Figure S12b in Supporting Information S1) by 0.13° latitude per decade ($P < 0.1$). In the North Pacific, the winter lysis latitude has significantly moved poleward by 0.10° latitude per decade ($P < 0.05$), consistent with the longer and farther-reaching winter tracks shown in Figure 8. The cyclone radius has significantly increased only in autumn, by 6.4 km per decade in the Arctic

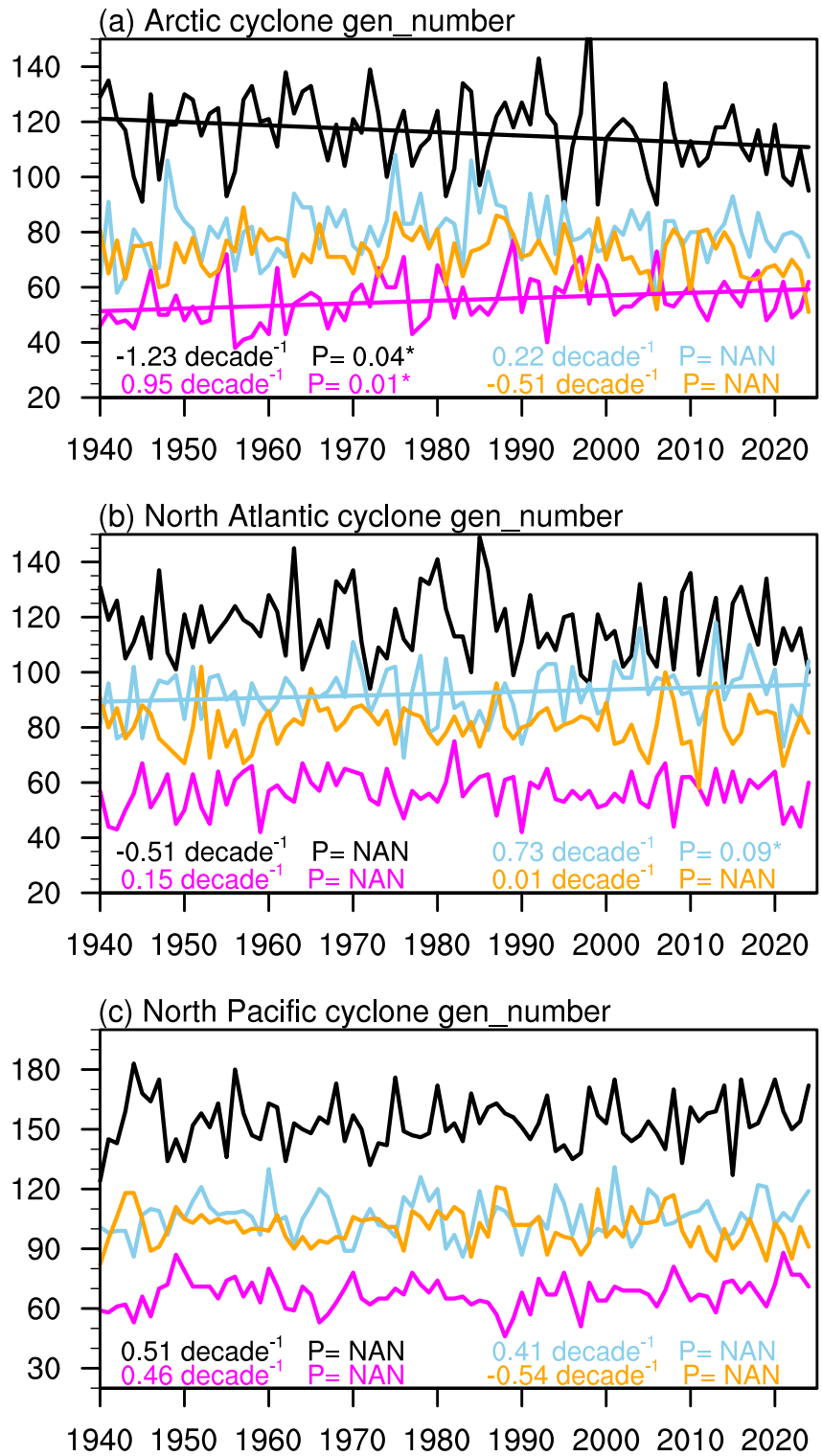

Figure 5. Time evolutions of seasonal cyclone generation number from 1940 to 2024 in the (a) Arctic, (b) North Atlantic, and (c) North Pacific, respectively. Black, sky blue, magenta, and orange lines denote winter (DJF), spring (MAM), summer (JJA), and autumn (SON), respectively. Regression coefficients are shown in corresponding colors, and significant levels (P values) are given with the asterisks denoting that the trends are significant at the 0.1 levels. Nonsignificant trends are marked as "NAN." Seasonal linear regressions are given by straight lines only for the significant time series. Specifically, the trends are -1.23 decade^{-1} for DJF ($P < 0.05$) and $+0.95$ decade^{-1} for JJA ($P < 0.05$) in the Arctic, and $+0.73$ decade^{-1} for MAM ($P < 0.1$) in the North Atlantic, respectively.

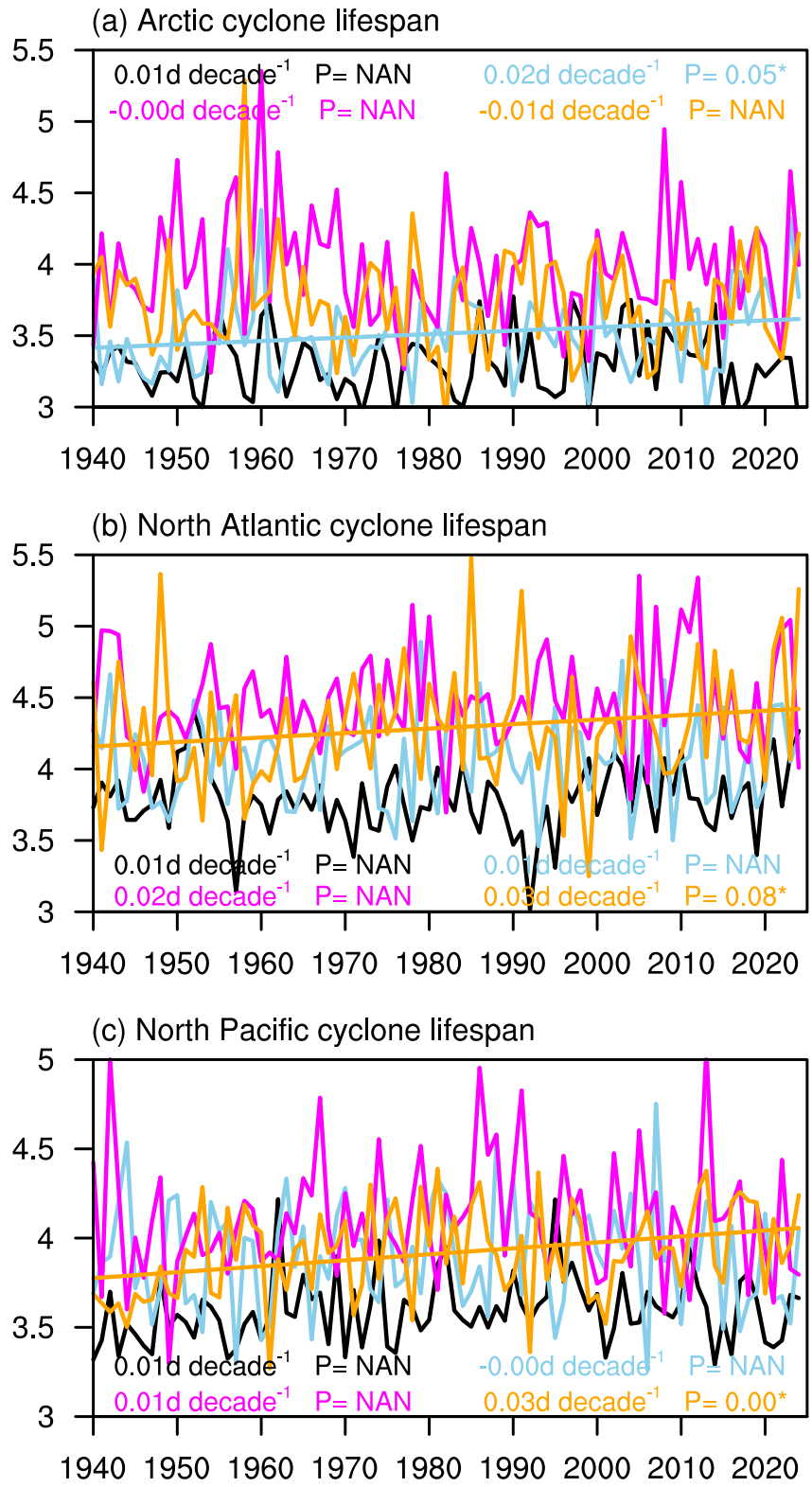

Figure 6. Same as Figure 5, but for cyclone lifespan (day). Specifically, the trends are +0.02 days decade^{-1} for MAM ($P < 0.05$) in the Arctic, +0.03 days decade^{-1} for SON ($P < 0.1$) in the North Atlantic, and +0.03 days decade^{-1} for SON ($P < 0.01$) in the North Pacific, respectively.

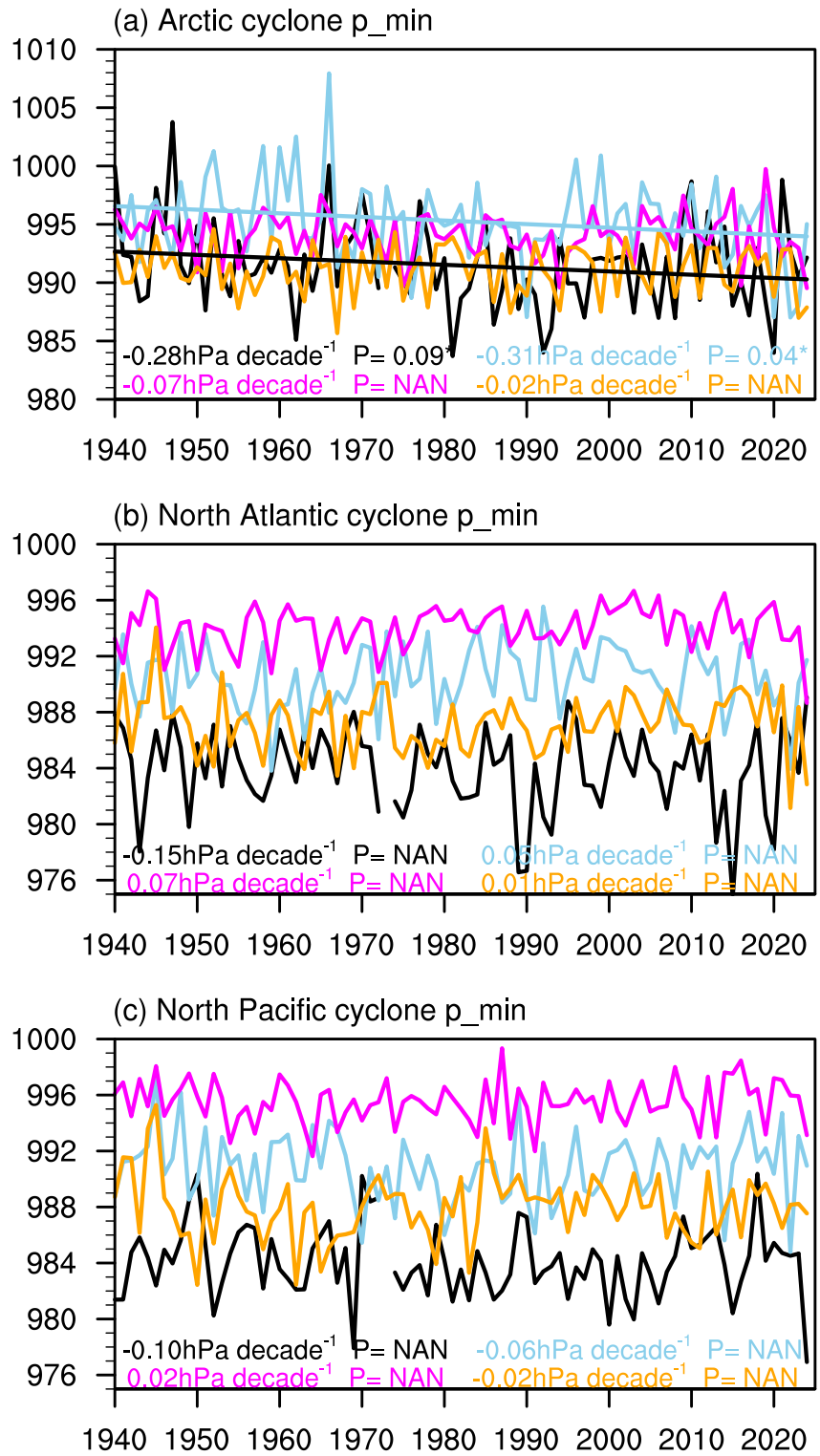

Figure 7. Same as Figure 5, but for cyclone central sea level pressure (hPa). Specifically, the trends are −0.28 hPa decade^{-1} for DJF ($P < 0.1$) and −0.31 hPa decade^{-1} for MAM ($P < 0.05$) in the Arctic, respectively.

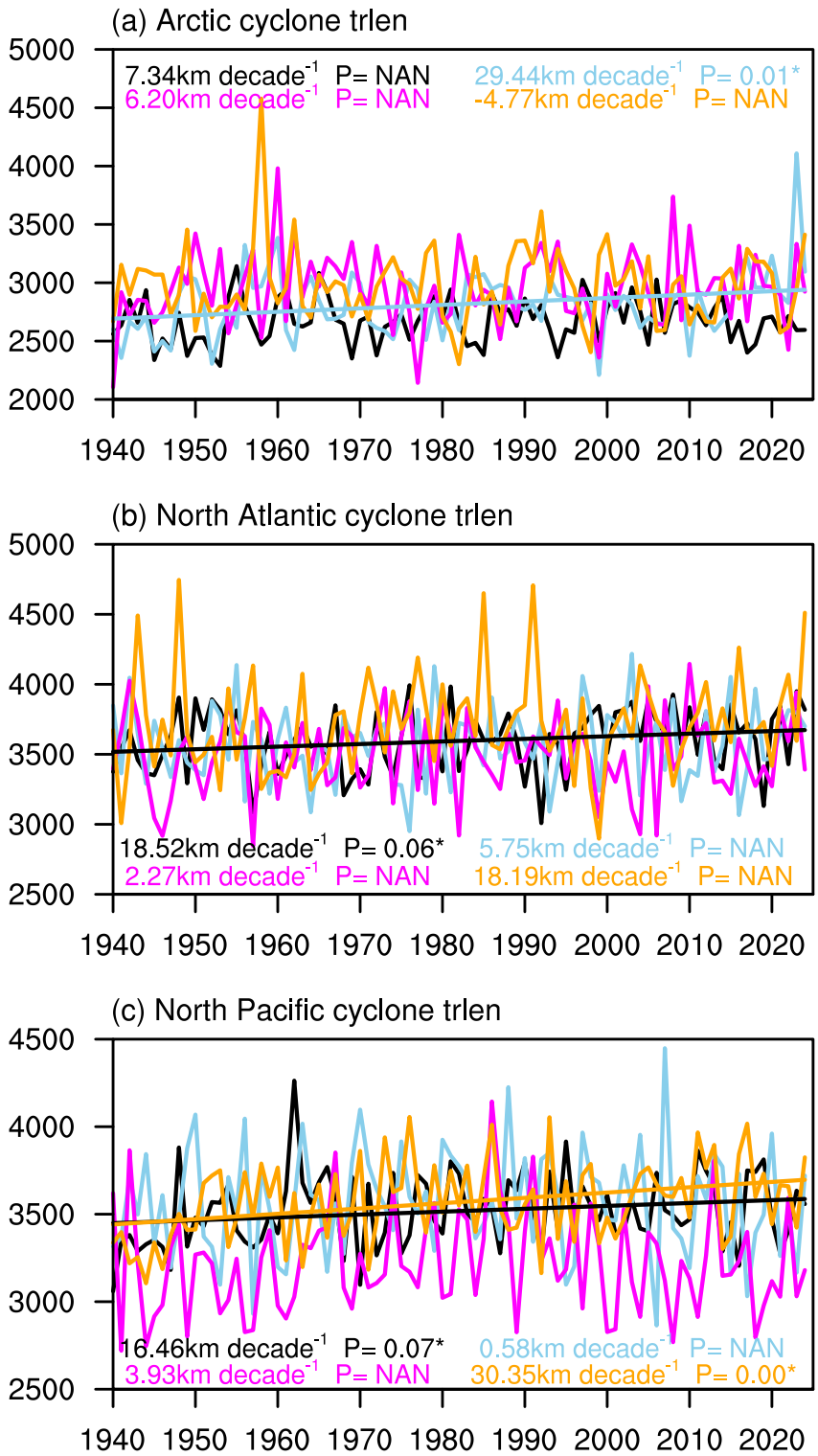

Figure 8. Same as Figure 5, but for cyclone trajectory length (km). Specifically, the trends are +29.44 km decade^{-1} for MAM ($P < 0.05$) in the Arctic, +18.52 km decade^{-1} for DJF ($P < 0.1$) in the North Atlantic, and +16.46 km decade^{-1} for DJF ($P < 0.1$) and +30.35 km decade^{-1} for SON ($P < 0.01$) in the North Pacific.

Table 1
Summary of the Significant Trends of Seasonal Cyclone Metrics in the Arctic, North Atlantic, and North Pacific

		DJF	MAM	JJA	SON
gen_num (decade^{-1})	Arctic	−1.23**		0.95***	
	NA		0.73*		
	NP				
lifespan (d decade^{-1})	Arctic		0.02**		
	NA				0.03*
	NP				0.03***
p_min (hPa decade^{-1})	Arctic	−0.28*	−0.31**		
	NA				
	NP				
trlen (km decade^{-1})	Arctic		29.44***		
	NA	18.52*			
	NP	16.46*			30.35***
lat_gen (° decade^{-1})	Arctic				
	NA			−0.1*	
	NP				
lat_lys (° decade^{-1})	Arctic				
	NA			−0.13*	
	NP	0.1**			
radius (km decade^{-1})	Arctic				6.43**
	NA				
	NP				10.37***

Note. The single, double, and triple asterisks after the numbers represent the trends are significant at the 0.1, 0.05, and 0.01 levels, respectively.

(Figure S13a in Supporting Information S1) and 10.37 km per decade in the North Pacific (Figure S13c in Supporting Information S1) ($P < 0.05$).

Considering a lot of the trends are patchy and localized in the North Atlantic and North Pacific, we further repeat the analysis for the core storm track belts in the North Atlantic (60°W–0°E, 45°–65°N) and North Pacific (140°-E−130°W, 45°–65°N). We observe nearly no significant trend for the Atlantic storm track region (Figure S14 in Supporting Information S1), while the autumn lifespan and track length are consistent in both the basin-wide and the Pacific storm track regions (Figure S15 in Supporting Information S1). However, interpreting these local differences rigorously would require tracking the decadal meridional and zonal shifts of the storm-track axis itself and separating storms that migrate into or out of a moving storm-track frame, which should be studied in the future.

Together, this section depicts a patchwork of season-specific and basin-specific adjustments rather than a uniform hemispheric trend. Table 1 summarizes the significant trends of cyclone metrics in the Arctic, North Atlantic, and North Pacific, respectively. The Arctic winter cyclone genesis count is declining, while the deepest winter and spring cyclones are intensifying, and spring systems also live longer and travel farther. Combined with the increasing Arctic cyclone track density trends in Figure 2a, these indicate more extratropical cyclones from the North Atlantic and North Pacific into the Arctic, supplemented by enhanced local summer cyclogenesis and larger autumn cyclones. The North Atlantic is experiencing significant lengthening of cyclone tracks in winter, more cyclogenesis in spring, equatorward retreat of the summer cyclone belt, and longer cyclone lifespans in autumn. The North Pacific shows lengthening tracks and longer lifespans in autumn and winter, without a concurrent rise in storm counts.

4. Physical Mechanisms

To establish whether the changes in Section 3 are dynamically linked to the large-scale climatological changes, and to place the observed phenomena in the context of recent process studies (e.g., Bray & Cavallo, 2024; Crawford et al., 2022; Song et al., 2025), we first examine long-term trends in sea-ice concentration (SIC) and then quantify how the Arctic SIC trend modulates cyclone track density and intensity. Figure S16 in Supporting Information S1 confirms a basin-wide decline in SIC during 1940–2024, and the magnitude and footprint of the trend are season-dependent (Onarheim et al., 2018; Simmonds & Li, 2021; Stroeve & Notz, 2018). Winter (Figure S16a in Supporting Information S1) losses remain confined to the marginal-ice zone (−2.5% to −5% decade^{-1}), whereas spring (Figure S16b in Supporting Information S1) trends penetrate farther into the central Arctic. By summer and autumn (Figures S16c and S16d in Supporting Information S1) the signal becomes pervasive, coherent reductions of −5% to −10% per decade blanket almost the entire Arctic Ocean, and the areal extent of significant negative trends more than doubles relative to winter (Figure S16a in Supporting Information S1). These patterns suggest that the ice–ocean–atmosphere interface has expanded poleward, resulting in a substantially different baroclinic backdrop for the present-day cyclones (Screen et al., 2018).

Figure 9 links the SIC decrease to cyclone intensity, and the regression maps are highly correlated with the long-term trends of seasonal cyclone intensity (Figure 4). The regression field is dominated by significant negative coefficients over the central Arctic in winter and spring (Figures 9a and 9b), implying that cyclones that penetrate open water deepen more than expected. Physically, sea ice modifies this in two main ways: one is the insulation effect and the other is enhanced heat storage and release after sea ice retreats (Maykut & Untersteiner, 1971; Screen & Simmonds, 2010; Serreze & Barry, 2011). The ice pack reflects a significant portion of the incoming solar radiation and limits conductive and turbulent heat transfer. As a result, the near-surface air temperature tends to follow the cold ice-surface temperature, and the effective temperature difference that drives air–sea heat exchange is small. When sea ice retreats, the upper ocean absorbs more solar radiation. The heat is stored in the

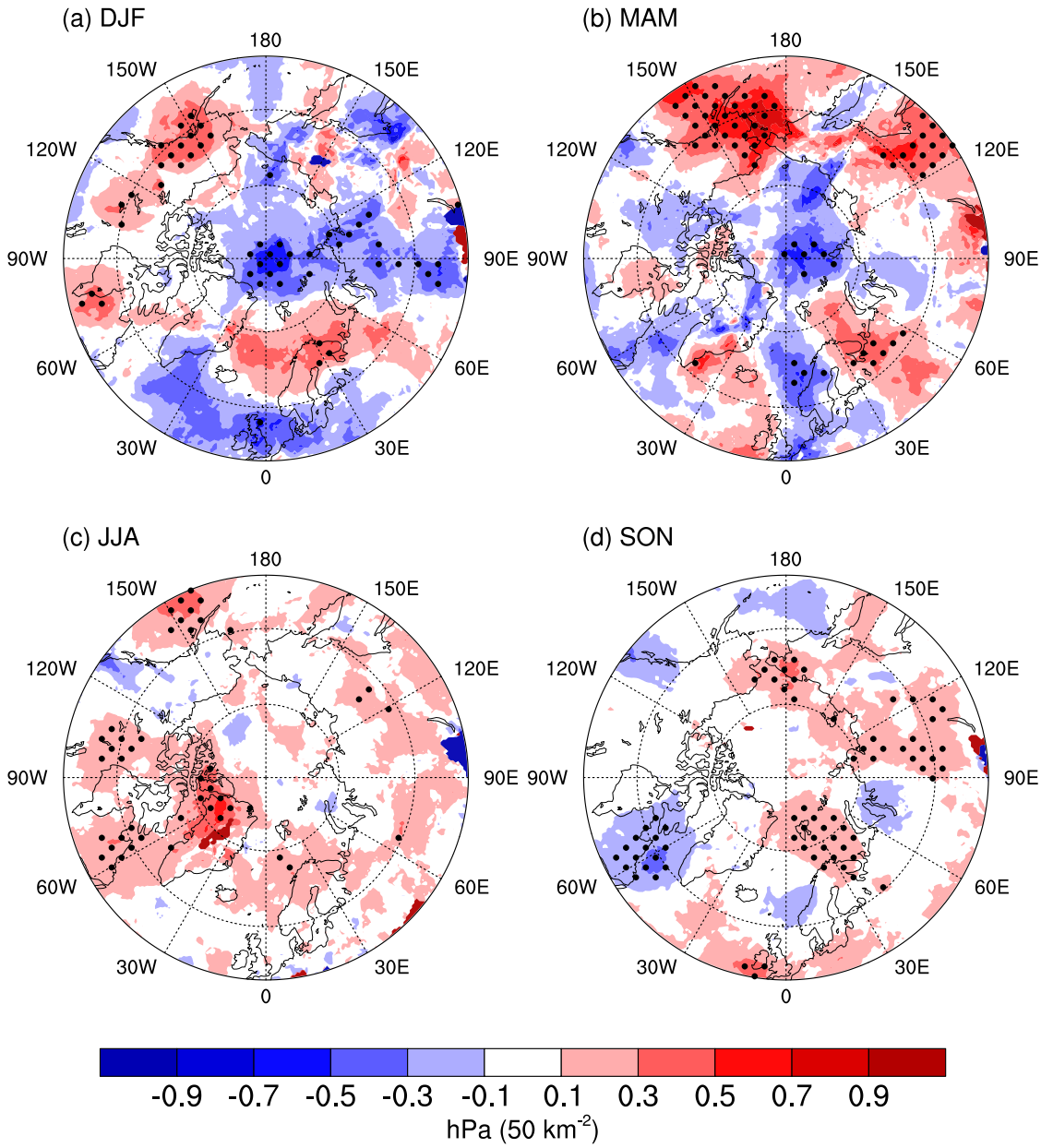

Figure 9. Regression distributions of cyclone intensity (hPa) anomalies against the average Arctic sea ice concentration from 1940 to 2024 in (a) winter (DJF), (b) spring (MAM), (c) summer (JJA), and (d) autumn (SON), respectively. Black dots denote that the regression coefficients are significant at the 0.05 levels.

mixed layer rather than being consumed by melting ice. The relatively warm ocean is directly exposed to cold air, and the temperature contrast between the sea surface and near-surface air likewise increases. This finding echoes the surface-flux mechanism articulated by several past studies, that decreased ice cover enhances upward sensible and latent heat fluxes (Rinke et al., 2006; Screen & Simmonds, 2010), weakens static stability (Jaiser et al., 2012; Koyama et al., 2017) and accelerates baroclinic growth (Crawford et al., 2022). A recent work emphasizes that the winter sea-ice–storm-track relationship can be regime dependent and not strictly unidirectional, with some years showing primarily atmosphere-driven coupling (Mousavizadeh et al., 2025). We therefore interpret Figure 9 as quantifying sea-ice–cyclone co-variability consistent with the surface-flux/baroclinicity mechanism, while recognizing that the direction of influence may vary. In summer and autumn (Figures 9c and 9d), the negative regressions over the Arctic disappear, and the overall regressions are much weaker. These results indicate that the long-term trend toward more intense cyclones in response to Arctic SIC reduction primarily occurs in winter and spring.

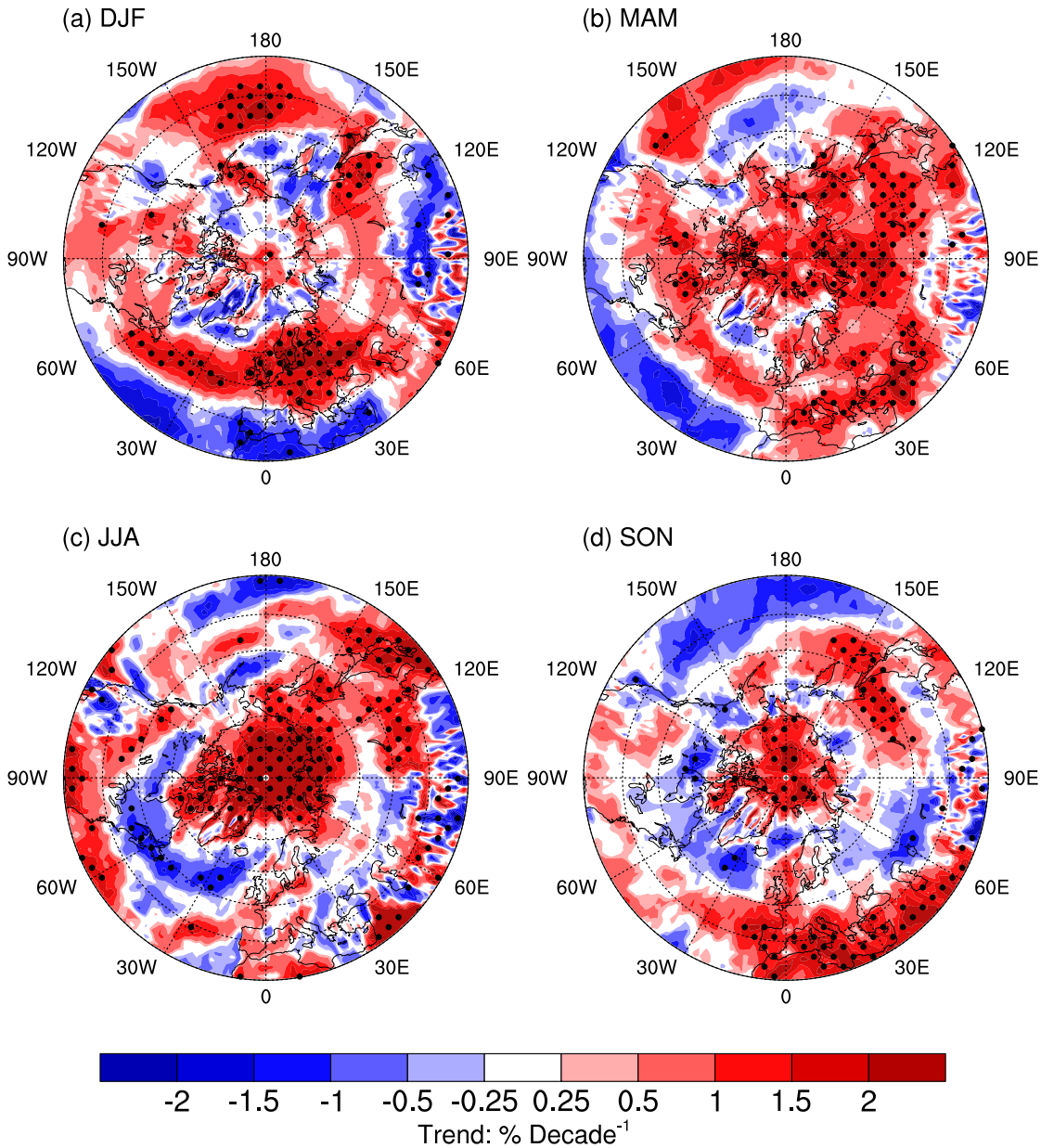

Figure 10. Spatial distributions of the relative 850 hPa Eady growth rate trend (trend/climatology) (% decade^{-1}) of extratropical and Arctic cyclones in (a) winter (DJF), (b) spring (MAM), (c) summer (JJA), and (d) autumn (SON), respectively. Black dots denote that the trends are significant at the 0.05 levels.

Considering that diminishing sea-ice concentration modulates cyclone deepening through enhanced surface heat fluxes, the next question is whether those flux-driven thermodynamic changes translate into a large-scale dynamic environment more favorable to baroclinic growth. The lower-tropospheric EGR provides exactly that diagnostic because it combines static stability with vertical wind shear (Crawford et al., 2022; Hoskins & Valdes, 1990). For the climate mean state (Figure S17 in Supporting Information S1), the highest oceanic EGR values trace the familiar North Atlantic and North Pacific storm tracks, while the central Arctic remains comparatively baroclinically quiet. Long-term trends of seasonal 850 hPa EGR (Figure 10) also have similar patterns to Figure 4. In winter (Figure 10a), the largest positive EGR trends appear well south of the ice edge. The central Arctic, by contrast, shows little change. By summer (Figure 10c) the pattern reverses, a strengthening EGR migrates into the central Arctic as SIC reaches its minimum, which coincides with the increasing and deepening Arctic cyclones (Figures 4a and 5a). Spring (Figure 10b) shows a strengthening trend surrounding the North Pole, matching the appearance of deeper spring cyclones (Figure 7a). Autumn (Figure 10d) maintains an Arctic centered positive

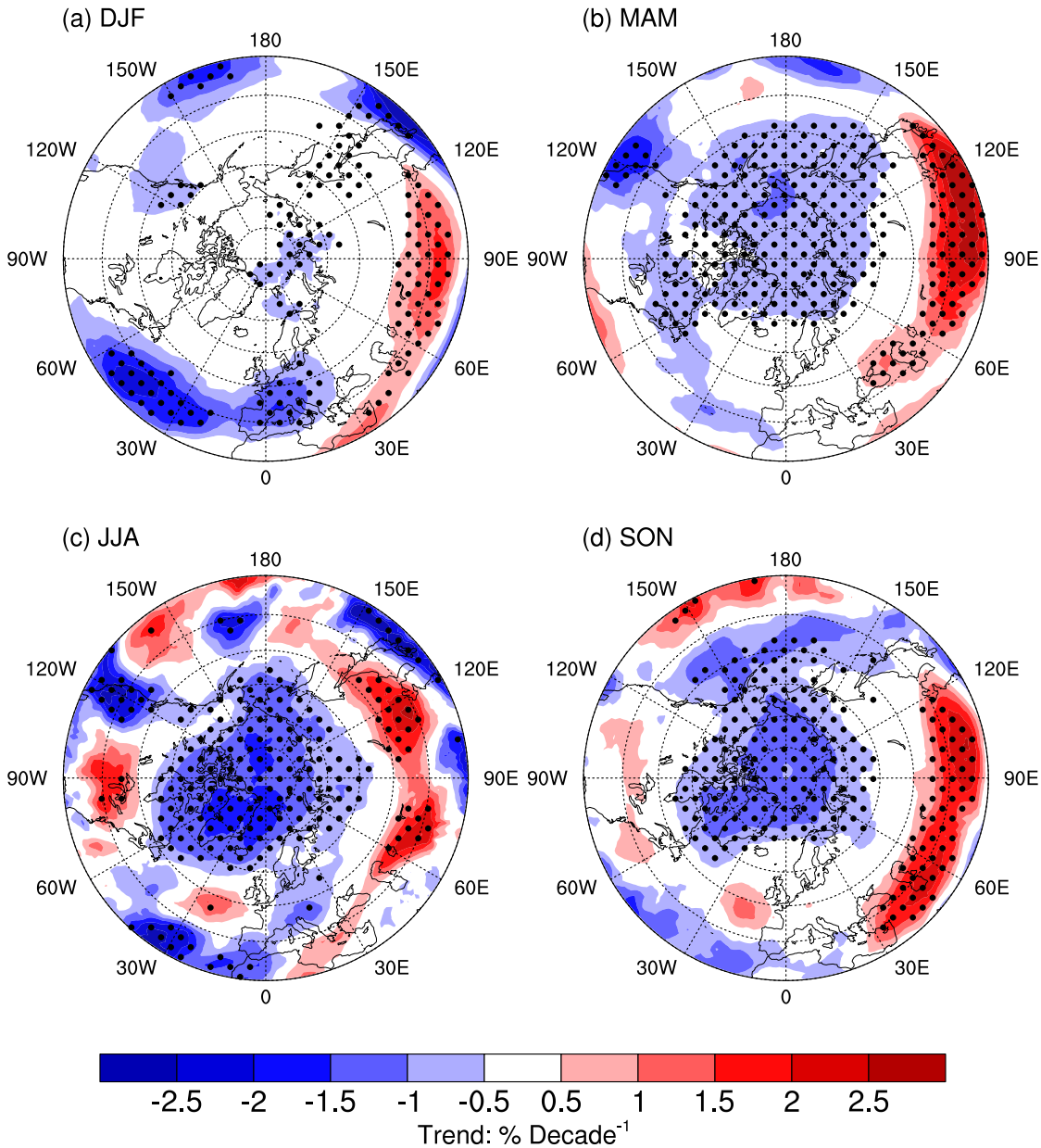

Figure 11. Spatial distributions of the relative 200 hPa potential vorticity trend (trend/climatology) (% decade^{-1}) of extratropical and Arctic cyclones in (a) winter (DJF), (b) spring (MAM), (c) summer (JJA), and (d) autumn (SON), respectively. Black dots denote that the trends are significant at the 0.05 levels.

core, though weaker than in summer. The phenomena of seasonal EGR migration trends play a dynamic bridge between the Arctic sea-ice loss and the cyclone deepening.

High-latitude cyclone behavior is also sensitive to the upper-tropospheric potential vorticity (PV) field because the meridional gradient of PV controls jet strength and therefore the latitude to which baroclinic waves can propagate. Figure S18 in Supporting Information S1 depicts a dome of 200 hPa PV over the Arctic and a sharp radial drop between 60°N and 70°N that coincides with the climatological jet core. In winter (Figure 11a), the largest positive PV trends lie along the western boundary-current sectors of the North Atlantic and North Pacific. This marginally steepens the PV gradient on the equator-side of the climatological jet. The pattern favors the subtropical EGR increase and the weak Arctic EGR signal (Figure 10a) and explains why winter cyclone activity has become more vigorous in mid-latitudes (Figure 4a). From spring through autumn (Figures 11b–11d), the trends are different, with significant PV decreases broadly across the central Arctic. The result is a systematic

decrease in the meridional PV gradient where sea ice has retreated most and where EGR has strengthened. A weaker gradient lowers the dynamic barrier that usually confines Rossby waves and mature cyclones to mid-latitudes (Bray & Cavallo, 2024; Čampa & Wernli, 2012). The coincidence of (a) negative PV-gradient trends, (b) positive low-level EGR trends, and (c) the strongest increases in cyclone intensity allows us to expand on the findings of Crawford et al. (2022) in two ways. First, it shows that when taking a longer time series (1940–2024), the connection between sea ice loss, greater low-level baroclinicity, and enhanced cyclone intensification is more apparent even in summer and autumn. Second, it demonstrates another driver of Arctic cyclone changes with the PV trends driving the increased poleward migration of cyclones. Sea-ice loss raises baroclinicity, and—by flattening the upper-level PV dome—removes the jet-level constraint on poleward cyclone migration (Tamarin and Kaspi, 2017). However, although changes in low-level EGR and upper-level PV gradients can influence the steering airflow, the basin-mean cyclone translation speed mostly exhibits weak trends (Figure S10 in Supporting Information S1).

As an additional first-order quantification of the proposed pathway, we constructed basin-mean seasonal time series over 1940–2024 for SIC, 850 hPa EGR, 200 hPa meridional PV gradient magnitude ($|\partial PV/\partial y|$), and a meridional migration proxy ($\Delta\varphi$) defined as the difference between the mean lysis and genesis latitudes. Using least-squares regressions, the SIC–EGR linkage was most robust in the Arctic warm seasons, with significant anticorrelations in MAM ($r = -0.29$, $P < 0.01$) and JJA ($r = -0.56$, $P < 0.01$). In Arctic JJA, EGR also covaries significantly with $|\partial PV/\partial y|$ ($r = -0.43$, $P < 0.01$), and over the North Pacific, the EGR – $|\partial PV/\partial y|$ relationship is most evident in the cold season (e.g., DJF $r = 0.42$, $P < 0.01$; SON $r = 0.41$, $P < 0.01$). Finally, in the North Pacific DJF, $|\partial PV/\partial y|$ is significantly related to $\Delta\varphi$ ($r = 0.32$, $P < 0.01$), consistent with the notion that changes in upper-level PV structure can modulate the seasonal expression of storm track migration.

Taken together, Arctic sea-ice loss increases the air–sea temperature contrast along the marginal-ice zone and over the Arctic Ocean. This favors larger lower-tropospheric EGR on the poleward flanks of the North Atlantic and North Pacific storm tracks and in newly ice-free seas, providing a more baroclinic environment in which cyclones can deepen more efficiently, maintain their intensity for longer and form more frequently within the Arctic basin. At the same time, the weakening of the upper-tropospheric PV dome over the Arctic reduces the jet-level barrier between mid-latitudes and high-latitudes and thus facilitates the poleward migration and maintenance of extratropical cyclones.

Although our interpretation focuses on the long-term, physically consistent linkage between Arctic SIC decline, enhanced lower-tropospheric baroclinicity (EGR), and concurrent changes in upper-level PV structure, cyclone statistics also exhibit substantial interannual-to-decadal variability. Part of this variability reflects large-scale climate modes that modulate the eddy-driven jet and storm tracks. For example, North Atlantic Oscillation/Arctic Oscillation-related variability can shift the North Atlantic storm track latitude and influence the frequency and pathways of cyclones entering the Arctic (Thompson & Wallace, 1998; Woollings et al., 2010). Pacific decadal oscillation can alter the Aleutian Low and the North Pacific storm track entrance (Newman et al., 2016). These modes therefore amplify or offset the long-term forced signal over particular decades and may contribute to the spatially patchy trend patterns in some seasons. A dedicated separation of forced trends from internal variability is beyond the scope of this study, but we note these influences here to contextualize the long-term changes reported above.

5. Conclusions

Using the ERA5 reanalysis data set spanning 1940 to 2024, we analyzed cyclone characteristics across four seasons and three major ocean basins, revealing a multi-decadal reshaping of NH marine cyclone activity. Since 1940, cyclone activity has become more frequent and significantly more intense over the central Arctic Ocean. Extratropical cyclone intensity has also increased in the central North Pacific during winter and summer, and in the North Atlantic storm track region during spring and autumn.

Basin-wide averages show a decline in Arctic cyclone genesis during winter, despite increasing intensity, while summer genesis has increased. Spring Arctic cyclones, often overlooked in previous studies, now show higher intensity, longer lifespans, and more extended tracks. In the North Atlantic, cyclone tracks have lengthened in winter, genesis has increased in spring, and storm lifespans have grown in autumn. In the North Pacific, cyclone paths have become longer in winter, and autumn storms have become notably larger, longer-lived, and more wide-ranging.

Our winter results align with those of Karwat et al. (2022), who reported a long-term increase in winter extratropical cyclone intensity, lifespan, and track length. The comparison of the three reanalysis data sets also increased the robustness of the results. This consistency across studies, despite differences in cyclone detection methods, supports the robustness of our findings and adds confidence in assessing cyclone changes beyond winter—especially in the understudied spring and autumn seasons.

The spatial and seasonal patterns observed are physically consistent with coupled changes from the surface to the upper troposphere. Areas with the greatest SIC loss also showed enhanced lower-tropospheric baroclinicity and negative correlations between SIC and cyclone intensity. As sea ice retreats, the EGR at 850 hPa increases across the central Arctic from spring through autumn, while the upper-tropospheric (200 hPa) potential vorticity gradient weakens north of 70°N. These changes reduce static stability, promote baroclinic development, and lower the jet-level barrier to poleward cyclone propagation.

Together, this evidence indicates that long-term climate change, particularly Arctic amplification, is already modifying NH cyclone behavior well beyond the traditionally emphasized winter and summer extremes (Screen et al., 2018). These findings underscore the need for climate forecasts and projections to treat spring and autumn cyclone activity with the same level of scrutiny long given to winter and summer.

Conflict of Interest

The authors declare no conflicts of interest relevant to this study.

Data Availability Statement

ERA5 data are provided by the Climate Data Store (https://cds.climate.copernicus.eu/datasets/reanalysis-era5-pressure-levels-monthly-means?tab=overview). JRA55 data are provided by the Geoscience Data Exchange (https://gdex.ucar.edu/datasets/d628000/). NOAA20C-V3 data are provided by the Physical Sciences Laboratory (https://psl.noaa.gov/data/gridded/data.20thC_ReanV3.html). HadiSST is provided by the Met Office Hadley Centre (https://www.metoffice.gov.uk/hadobs/hadisst/).

Acknowledgments
This work is supported by Tsinghua University (100008001) and Swedish Formas (2020-00982 and 2023-01648). Z.L. is supported by Stiftelsen Lars Hiertas Minne (FO2025-0139). A.C. receives funding from the Canadian National Sciences and Engineering Research Council (DGECR-2025-00045).

References

Barnes, E. A., & Screen, J. A. (2015). The impact of Arctic warming on the midlatitude jet-stream: Can it? Has it? Will it? *Wiley Interdisciplinary Reviews: Climate Change*, *6*(3), 277–286. https://doi.org/10.1002/wcc.337

Bengtsson, L., Hodges, K. I., & Roeckner, E. (2006). Storm tracks and climate change. *Journal of Climate*, *19*(15), 3518–3543. https://doi.org/10.1175/JCLI3815.1

Blackport, R., & Screen, J. A. (2020). Weakened evidence for mid-latitude impacts of Arctic warming. *Nature Climate Change*, *10*(12), 1065–1066. https://doi.org/10.1038/s41558-020-00954-y

Bray, M. T., & Cavallo, S. M. (2024). Investigating Arctic cyclone–tropopause polar vortex interactions with idealized observing system simulation experiments. *Monthly Weather Review*, *152*(7), 1445–1467. https://doi.org/10.1175/MWR-D-23-0215.1

Čampa, J., & Wernli, H. (2012). A PV perspective on the vertical structure of mature midlatitude cyclones in the Northern Hemisphere. *Journal of the Atmospheric Sciences*, *69*(2), 725–740. https://doi.org/10.1175/JAS-D-11-050.1

Chang, E. K. M., Ma, C.-G., Zheng, C., & Yau, A. M. W. (2016). Observed and projected decrease in Northern Hemisphere extratropical cyclone activity in summer and its impacts on maximum temperature. *Geophysical Research Letters*, *43*(5), 2200–2208. https://doi.org/10.1002/2016GL068172

Chen, S., Chen, W., Yu, B., Wu, L., Chen, L., Li, Z., et al. (2023). Impact of the winter Arctic sea ice anomaly on the following summer tropical cyclone genesis frequency over the western North Pacific. *Climate Dynamics*, *61*(7–8), 3971–3988. https://doi.org/10.1007/s00382-023-06789-5

Crawford, A. D., Lukovich, J. V., McCrystall, M. R., Stroeve, J. C., & Barber, D. G. (2022). Reduced sea ice enhances intensification of winter storms over the Arctic Ocean. *Journal of Climate*, *35*(11), 3353–3370. https://doi.org/10.1175/JCLI-D-21-0747.1

Crawford, A. D., Schreiber, E. A. P., Sommer, N., Serreze, M. C., Stroeve, J. C., & Barber, D. G. (2021). Sensitivity of Northern Hemisphere cyclone detection and tracking results to fine spatial and temporal resolution using ERA5. *Monthly Weather Review*, *149*(8), 2581–2598. https://doi.org/10.1175/MWR-D-20-0417.1

Crawford, A. D., & Serreze, M. C. (2016). Does the summer Arctic frontal zone influence Arctic Ocean cyclone activity? *Journal of Climate*, *29*(13), 4977–4993. https://doi.org/10.1175/JCLI-D-15-0755.1

Dzambo, A., McFarquhar, G., Sledd, A., & L'Ecuyer, T. (2023). Assessing latent and kinetic energy trend changes in extratropical cyclones from 1940 to 2020: Results from ERA-5 reanalysis. *Geophysical Research Letters*, *50*(23), e2023GL105207. https://doi.org/10.1029/2023GL105207

Eady, E. T. (1949). Long waves and cyclone waves. *Tellus*, *1A*(3), 33–52. https://doi.org/10.1111/j.2153-3490.1949.tb01265.x

Feser, F., Barcikowska, M., Krueger, O., Schenk, F., Weisse, R., & Xia, L. (2014). Storminess over the North Atlantic and north-western Europe: A review. *Quarterly Journal of the Royal Meteorological Society*, *141*(687), 350–382. https://doi.org/10.1002/qj.2364

Francis, J. A., & Vavrus, S. J. (2012). Evidence linking Arctic amplification to extreme weather in mid-latitudes. *Geophysical Research Letters*, *39*(6), L06801. https://doi.org/10.1029/2012GL051000

Gray, S. L., Hodges, K. I., Vautrey, J. L., & Methven, J. (2021). The role of tropopause polar vortices in the intensification of summer Arctic cyclones. *Weather and Climate Dynamics*, *2*(4), 1303–1324. https://doi.org/10.5194/wcd-2-1303-2021

Hay, S., Priestley, M. D. K., Yu, H., Catto, J. L., & Screen, J. A. (2023). The effect of Arctic sea-ice loss on extratropical cyclones. *Geophysical Research Letters*, *50*(17), e2023GL102840. https://doi.org/10.1029/2023GL102840

Hermoso, A., Riviere, G., Harvey, B., Methven, J., & Schemm, S. (2024). A dynamical interpretation of the intensification of the winter North Atlantic jet stream in reanalysis. *Journal of Climate*, *37*(22), 5853–5881. https://doi.org/10.1175/JCLI-D-23-0757.1

Hersbach, H., Bell, B., Berrisford, P., Hirahara, S., Horanyi, A., Munoz-Sabater, J., et al. (2020). The ERA5 global reanalysis [Dataset]. *Quarterly Journal of the Royal Meteorological Society*, *146*(730), 1999–2049. https://doi.org/10.1002/qj.3803

Hoskins, B. J., & Hodges, K. I. (2002). New perspectives on the Northern Hemisphere winter storm tracks. *Journal of the Atmospheric Sciences*, *59*(6), 1041–1061. https://doi.org/10.1175/1520-0469(2002)059<1041:NPOTNH>2.0.CO;2

Hoskins, B. J., & Valdes, P. J. (1990). On the existence of storm tracks. *Journal of the Atmospheric Sciences*, *47*(15), 1854–1864. https://doi.org/10.1175/1520-0469(1990)047<1854:OTEOST>2.0.CO;2

Hsu, P.-C., Hsu, H.-H., Hong, H.-J., & Chen, Y.-T. (2025). Subtropical warming enhances North Pacific midlatitude winter storm track activity in recent decades. *npj Climate and Atmospheric Science*, *8*(1), 235. https://doi.org/10.1038/s41612-025-01108-7

IPCC. (2022). In V. Masson-Delmotte, P. Zhai, A. Pirani, S. L. Connors, C. Péan, et al. (Eds.), *Climate change 2021: The physical science basis. Contribution of working group I to the sixth assessment report of the intergovernmental panel on climate change*. Cambridge University Press. Retrieved from https://www.ipcc.ch/report/ar6/wg1/

Jaiser, R., Dethloff, K., Handorf, D., & Cohen, J. (2012). Impact of sea ice cover changes on the Northern Hemisphere atmospheric winter circulation. *Tellus*, *64*(1), 11575. https://doi.org/10.3402/tellusa.v64i0.11595

Karwat, A., Franzke, C. L. E., & Blender, R. (2022). Long-term trends of Northern-Hemispheric winter cyclones in the extended ERA5 reanalysis. *Journal of Geophysical Research: Atmospheres*, *127*(22), e2022JD036952. https://doi.org/10.1029/2022JD036952

Kenigson, J. S., & Timmermans, M.-L. (2021). Arctic cyclone activity and the Beaufort high. *Journal of Climate*, *34*(10), 4119–4127. https://doi.org/10.1175/JCLI-D-20-0771.1

Kobayashi, S., Ota, Y., Harada, Y., Ebita, A., Moriya, M., Onoda, H., et al. (2015). The JRA-55 reanalysis: General specifications and basic characteristics. *Journal of the Meteorological Society of Japan. Series II*, *93*(1), 5–48. https://doi.org/10.2151/jmsj.2015-001

Koyama, T., Stroeve, J., Cassano, J., & Crawford, A. D. (2017). Sea ice loss and Arctic cyclone activity from 1979 to 2014. *Journal of Climate*, *30*(12), 4735–4754. https://doi.org/10.1175/jcli-d-16-0542.1

LeDrew, E. F. (1984). The role of local heat sources in synoptic activity within the polar basin. *Atmosphere-Ocean*, *22*(3), 309–327. https://doi.org/10.1080/07055900.1984.9649201

Lembo, V., Fabiano, F., Galfi, V. M., Graversen, R. G., Lucarini, V., & Messori, G. (2022). Meridional-energy-transport extremes and the general circulation of Northern Hemisphere mid-latitudes: Dominant weather regimes and preferred zonal wavenumbers. *Weather and Climate Dynamics*, *3*(3), 1037–1062. https://doi.org/10.5194/wcd-3-1037-2022

Lembo, V., Messori, G., Graversen, R., & Lucarini, V. (2019). Spectral decomposition and extremes of atmospheric meridional energy transport in the Northern Hemisphere midlatitudes. *Geophysical Research Letters*, *46*(13), 7602–7613. https://doi.org/10.1029/2019GL082105

Maykut, G. A., & Untersteiner, N. (1971). Some results from a time-dependent thermodynamic model of sea ice. *Journal of Geophysical Research*, *76*(6), 1550–1575. https://doi.org/10.1029/JC076i006p01550

Messori, G., & Czaja, A. (2012). On the sporadic nature of meridional heat transport by transient eddies. *Quarterly Journal of the Royal Meteorological Society*, *137*(673), 999–1008. https://doi.org/10.1002/qj.2011

Mousavizadeh, M., Alizadeh, O., Hodges, K. I., & Simmonds, I. (2025). Causality in the winter interaction between extratropical storm tracks, atmospheric circulation, and Arctic sea ice loss. *Journal of Geophysical Research: Atmospheres*, *130*(5), e2024JD042128. https://doi.org/10.1029/2024JD042128

Neu, U., Akperov, M. G., Bellenbaum, N., Benestad, R., Blender, R., Caballero, R., et al. (2013). IMILAST: A community effort to intercompare extratropical cyclone detection and tracking algorithms. *Bulletin of the American Meteorological Society*, *94*(4), 529–547. https://doi.org/10.1175/BAMS-D-11-00154.1

Newman, M., Alexander, M. A., Ault, T. R., Cobb, K. M., Deser, C., Lorenzo, E. D., et al. (2016). The Pacific decadal oscillation, revisited. *Journal of Climate*, *29*(12), 4399–4427. https://doi.org/10.1175/JCLI-D-15-0508.1

Onarheim, I. H., Eldevik, T., Smedsrud, L. H., & Stroeve, J. C. (2018). Seasonal and regional manifestation of Arctic sea ice loss. *Journal of Climate*, *31*(12), 4917–4932. https://doi.org/10.1175/JCLI-D-17-0427.1

Pierrehumbert, R. T., & Swanson, K. L. (1995). Baroclinic instability. *Annual Review of Fluid Mechanics*, *27*(1), 419–467. https://doi.org/10.1146/annurev.fl.27.010195.002223

Priestley, M. D., & Catto, J. L. (2022). Future changes in the extratropical storm tracks and cyclone intensity, wind speed, and structure. *Weather and Climate Dynamics*, *3*(1), 337–360. https://doi.org/10.5194/wcd-3-337-2022

Raible, C. C., Messmer, M., Lehner, F., Stocker, T. F., & Blender, R. (2018). Extratropical cyclone statistics during the last millennium and the 21st century. *Climate of the Past*, *14*(10), 1499–1514. https://doi.org/10.5194/cp-14-1499-2018

Raible, C. C., Pinto, J. G., Ludwig, P., & Messmer, M. (2020). A review of past changes in extratropical cyclones in the northern hemisphere and what can be learned for the future. *Wiley Interdisciplinary Reviews: Climate Change*, *12*(1), e680. https://doi.org/10.1002/wcc.680

Rayner, N. A., Parker, D. E., Horton, E. B., Folland, C. K., Alexander, L. V., Rowell, D. P., et al. (2003). Global analysis of sea surface temperature, sea ice, and night marine air temperature since the late nineteenth century. *Journal of Geophysical Research*, *108*(D14), 4407. https://doi.org/10.1029/2002JD002670

Rinke, A., Maslowski, W., Dethloff, K., & Clement, J. (2006). Influence of sea ice on the atmosphere: A study with an Arctic atmospheric regional climate model. *Journal of Geophysical Research: Atmosphere*, *111*(D16), D16103. https://doi.org/10.1029/2005JD006957

Rinke, A., Maturilli, M., Graham, R. M., Matthes, H., Handorf, D., Cohen, L., et al. (2017). Extreme cyclone events in the Arctic: Wintertime variability and trends. *Environmental Research Letters*, *12*(9), 094006. https://doi.org/10.1088/1748-9326/aa7def

Screen, J. A., Bracegirdle, T. J., & Simmonds, I. (2018). Polar climate change as manifest in atmospheric circulation. *Current Climate Change Reports*, *4*, 383–395. https://doi.org/10.1007/s40641-018-0111-4

Screen, J. A., & Simmonds, I. (2010). The central role of diminishing sea ice in recent Arctic temperature amplification. *Nature*, *464*(7293), 1334–1337. https://doi.org/10.1038/nature09051

Sepp, M., & Jaagus, J. (2011). Changes in the activity and tracks of Arctic cyclones. *Climate Change*, *105*(3–4), 577–595. https://doi.org/10.1007/s10584-010-9893-7

Serreze, M. C., & Barrett, A. P. (2008). The summer cyclone maximum over the central Arctic Ocean. *Journal of Climate*, *21*(5), 1048–1065. https://doi.org/10.1175/2007JCLI1810.1

Serreze, M. C., Barrett, A. P., Stroeve, J. C., Kindig, D. N., & Holland, M. M. (2009). The emergence of surface-based Arctic amplification. *The Cryosphere*, *3*(1), 11–19. https://doi.org/10.5194/tc-3-11-2009

Serreze, M. C., & Barry, R. G. (2011). Processes and impacts of Arctic amplification: A research synthesis. *Global and Planetary Change*, *77*(1–2), 85–96. https://doi.org/10.1016/j.gloplacha.2011.03.004

Serreze, M. C., Carse, F., Barry, R. G., & Rogers, J. C. (1997). Icelandic low cyclone activity: Climatological features, linkages with the NAO, and relationships with recent changes in the Northern Hemisphere circulation. *Journal of Climate*, *10*(3), 453–464. https://doi.org/10.1175/1520-0442(1997)010<0453:ILCACF>2.0.CO;2

Simmonds, I., Burke, C., & Keay, K. (2008). Arctic climate change as manifest in cyclone behavior. *Journal of Climate*, *21*(22), 5777–5796. https://doi.org/10.1175/2008JCLI2366.1

Simmonds, I., & Keay, K. (2000). Mean Southern Hemisphere extratropical cyclone behavior in the 40-Year NCEP–NCAR reanalysis. *Journal of Climate*, *13*(5), 873–885. https://doi.org/10.1175/1520-0442(2000)013<0873:MSHECB>2.0.CO;2

Simmonds, I., & Keay, K. (2009). Extraordinary September Arctic sea ice reductions and their relationships with storm behavior over 1979–2008. *Geophysical Research Letters*, *36*(19), L 19715. https://doi.org/10.1029/2009GL039810

Simmonds, I., & Li, M. (2021). Trends and variability in polar sea ice, global atmospheric circulations, and baroclinicity. *Annals of the New York Academy of Sciences*, *1504*(1), 167–186. https://doi.org/10.1111/nyas.14673

Simmonds, I., & Lim, E.-P. (2009). Biases in the calculation of Southern Hemisphere mean baroclinic eddy growth rate. *Geophysical Research Letters*, *36*(1), GL036320. https://doi.org/10.1029/2008GL036320

Simmonds, I., & Rudeva, I. (2012). The great Arctic cyclone of August 2012. *Geophysical Research Letters*, *39*(23), L23709. https://doi.org/10.1029/2012GL054259

Simmonds, I., & Rudeva, I. (2014). A comparison of tracking methods for extreme cyclones in the Arctic basin. *Tellus*, *66*(1), 25252. https://doi.org/10.3402/tellusa.v66.25252

Slivinski, L. C., Compo, G. P., Whitaker, J. S., Sardeshmukh, P. D., Giese, B. S., McColl, C., et al. (2019). Towards a more reliable historical reanalysis: Improvements for version 3 of the Twentieth century reanalysis system. *Quarterly Journal of the Royal Meteorological Society*, *154*(724), 2876–2908. https://doi.org/10.1002/qj.3598

Song, J.-N., Fu, G., Xu, Y., Han, Z., Sun, Q., & Wang, H. (2021). Assessment of the capability of CMIP6 global climate models to simulate Arctic cyclones. *Advances in Climate Change Research*, *12*(5), 660–676. https://doi.org/10.1016/j.accre.2021.07.007

Song, J.-N., Xu, Y., Han, Z., & Wu, J. (2025). CMIP6 projected trend of winter and summer variation in Arctic cyclones over the 21st century. *Climate Dynamics*, *63*(1), 82. https://doi.org/10.1007/s00382-024-07531-5

Stoll, P. J., Graversen, R. G., & Messori, G. (2023). The global atmospheric energy transport analysed by a wavelength-based scale separation. *Weather and Climate Dynamics*, *4*(1), 1–17. https://doi.org/10.5194/wcd-4-1-2023

Stroeve, J., & Notz, D. (2018). Change state of Arctic sea ice across all seasons. *Environmental Research Letters*, *13*(10), 103001. https://doi.org/10.1088/1748-9326/aade56

Tamarin-Brodsky, T., & Kaspi, Y. (2017). Enhanced poleward propagation of storms under climate change. *Nature Geoscience*, *10*(12), 908–913. https://doi.org/10.1038/s41561-017-0001-8

Tao, W., Zhang, J., Fu, Y., & Zhang, X. (2017). Driving roles of tropospheric and stratospheric thermal anomalies in intensification and persistence of the Arctic superstorm in 2012. *Geophysical Research Letters*, *44*(19), 10017–10025. https://doi.org/10.1002/2017GL074778

Thompson, D. W. J., & Wallace, J. M. (1998). The Arctic oscillation signature in the wintertime geopotential height and temperature fields. *Geophysical Research Letters*, *25*(9), 1297–1300. https://doi.org/10.1029/98GL00950

Ulbrich, U., Leckebusch, G. C., & Pinto, J. G. (2009). Extra-tropical cyclones in the present and future climate: A review. *Theoretical and Applied Climatology*, *96*(1–2), 117–131. https://doi.org/10.1007/s00704-008-0083-8

Vihma, T. (2014). Effects of Arctic sea-ice decline on weather and climate: A review. *Surveys in Geophysics*, *35*(5), 1175–1214. https://doi.org/10.1007/s10712-014-9284-0

Wallace, J. M., & Hobbs, P. V. (2006). In R. Dmowska, D. Hartmann, & H. T. Rossby (Eds.), *Atmospheric science: An introductory survey* (2nd ed.). Academic Press. (p. 483).

Wang, X., Swail, V. R., & Zwiers, F. W. (2006). Climatology and changes of extratropical cyclone activity: Comparison of ERA-40 with NCEP–NCAR reanalysis for 1958–2001. *Journal of Climate*, *19*(13), 3145–3166. https://doi.org/10.1175/JCLI3781.1

Wernli, H., & Schwierz, C. (2006). Surface cyclones in the ERA-40 dataset (1958–2001). Part I: Novel identification method and global climatology. *Journal of the Atmospheric Sciences*, *63*(10), 2486–2507. https://doi.org/10.1175/JAS3766.1

Wickström, S., Jonassen, M. O., Vihma, T., & Uotila, P. (2020). Trends in cyclones in the high-latitude North Atlantic during 1979–2016. *Quarterly Journal of the Royal Meteorological Society*, *146*(727), 762–779. https://doi.org/10.1002/qj.3707

Woollings, T., Hannachi, A., & Hoskins, B. (2010). Variability of the North Atlantic eddy-driven jet stream. *Quarterly Journal of the Royal Meteorological Society*, *136*(649), 856–868. https://doi.org/10.1002/qj.625

Yin, J. H. (2005). A consistent poleward shift of the storm tracks in simulations of twentieth- and twenty-first-century climate. *Geophysical Research Letters*, *32*(18), L18701. https://doi.org/10.1029/2005GL023684

Yu, B., Wang, X. L., Feng, Y., Chan, R., Compo, G. P., Slivinski, L. C., et al. (2022). Northern hemisphere extratropical cyclone activity in the twentieth century reanalysis version 3 (20CRv3) and its relationship with continental extreme temperatures. *Atmosphere*, *13*(8), 1166. https://doi.org/10.3390/atmos13081166

Zahn, M., Akperov, M., Rinke, A., Feser, F., & Mokhov, I. I. (2018). Trends of cyclone characteristics in the Arctic and their patterns from different reanalysis data. *Journal of Geophysical Research: Atmospheres*, *123*(5), 2737–2751. https://doi.org/10.1002/2017JD027439

Zhang, M., Perrie, W., & Long, Z. (2024). Impacts of climate change on Arctic winter cyclones. *Journal of Geophysical Research: Atmospheres*, *129*(24), e2024JD041503. https://doi.org/10.1029/2024JD041503

Zhang, X., Tang, H., Zhang, J., Walsh, J. E., Roesler, E. L., Hillman, B., et al. (2023). Arctic cyclones have become more intense and longer-lived over the past seven decades. *Communications Earth & Environment*, *4*(1), 348. https://doi.org/10.1038/s43247-023-01003-0

Zhang, X., Walsh, J. E., Zhang, J., Bhatt, U. S., & Ikena, M. (2004). Climatology and interannual variability of Arctic cyclone activity: 1948–2002. *Journal of Climate*, *17*(12), 2300–2317. https://doi.org/10.1175/1520-0442(2004)017<2300:CAIVOA>2.0.CO;2